INVERSE PROBLEMS FOR HEAT CONDUCTION EQUATION AND NAVIER-STOKES EQUATIONS

Ciałkowski M. and Frąckowiak A.
Technical University of Poznań, Chair of Thermal Engineering
Michal.Cialkowski@put.poznan.pl

Outline

1. MOTIVATION
2. FORMULATION OF THE PROBLEM
3. THE SOLUTION TO THE INVERSE PROBLEM
4. NUMERICAL CALCULATIONS
5. FINAL REMARKS

Warsaw 2010

INVERSE PROBLEMS

I. Design Problem (Cauchy Problem)

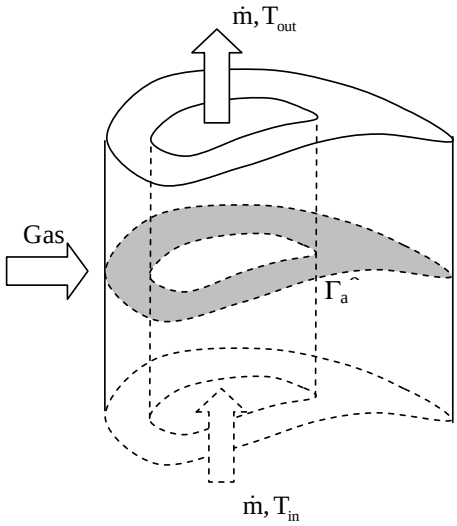

Given:

$\Delta T = 0, T\big|_{\Gamma_a}, q\big|_{\Gamma_a}$

Unknown:

$T\big|_{\Gamma_i}$

1. Application of inverse problem of the Poisson equation in the cooling process of a gas-turbine blade
2. A fitting algorithm for solving inverse problems of heat conduction, International Heat and Mass Transfer
3. Solution of Cauchy problem to stationary heat conduction equation by modified method of elementary balances with interpolation of the solution in physical plane, Inverse Problems in Science and Engineering

II. Boundary Inverse Probem

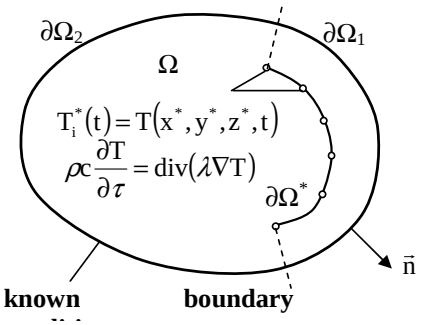

unknown:

a) T=?, I boundary condition

or

b) q=?, II boundary condition

or

c) α=?, III boundary condition

known: temperature distribution

$T_i^*(t) = T(x^*, y^*, z^*, t)$ choisen at points $(x^*, y^*, z^*) \in \partial\Omega^*$,

i=1,2,...,MP

III. Solution of Navier-Stokes Equation as inverse source problem

SOLUTION OF INVERSE DESIGN PROBLEM OF COOLING OF ANNULUS BY THE METHOD OF FUNDAMENTAL SOLUTIONS AND MINIMIZATION OF INTENSITY OF ENTROPY PRODUCTION

1.Motivation

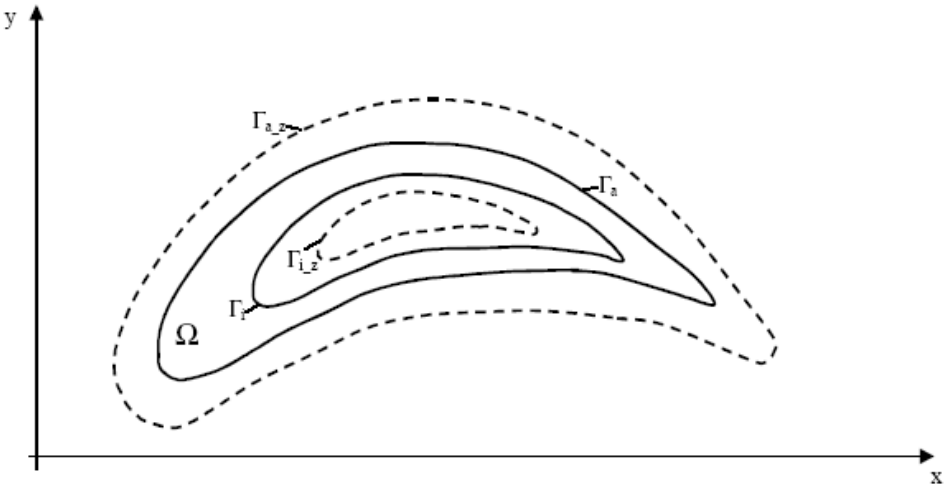

Fig. 1. Cooling blade; Γ_i, Γ_a – boundaries of blade, Γ_{i-z}, Γ_{a-z} – boundaries with distributed sources

2. FORMULATION OF PROBLEM

Consider a steady field of temperature, without sources, described by equation

$$div\left(\lambda(T)\nabla T\right)=0 \tag{1}$$

which by a Kirchoff transformation

$$u=\frac{1}{\lambda_0}\cdot\int_0^{T(x,y)}\lambda(\Theta)d\Theta=LT\quad,\quad \lambda_0=\lambda(0),\quad T=L^{-1}u \tag{2}$$

changes to a Laplace equation with an unknown temperature *u*

$$\Delta u=0 \tag{3}$$

For the before mentioned design problem we have

$$,\quad u\big|_{\Gamma_a}=f(x,y)\,,\ (x,y)\in\Gamma_a \tag{4}$$

$$\left.\frac{\partial u}{\partial n}\right|_{\Gamma_a}=q(x,y)\,,\quad (x,y)\in\Gamma_a \tag{5}$$

The solution of Eq (3) can be expressed in a form of a simple layer potential

$$\mathrm{u(x,y)}=\int_{\Gamma_{i-z}\cup\Gamma_{a-z}}\mathrm{p(\xi,\eta)}\cdot\underbrace{\ln\left[(\mathrm{x}-\xi)^2+(\mathrm{y}-\eta)^2\right]}_{\text{fundamental solution}}\mathrm{ds}\quad,$$

$$(x,y)\in\overline{\Omega}\,,\quad(\xi,\eta)\in\Gamma_{i-z}\cup\Gamma_{a-z} \tag{6}$$

with a condition

$$\int_{\Gamma_{i-z}\cup\Gamma_{a-z}}\mathrm{p(\xi,\eta)\,ds}=0$$

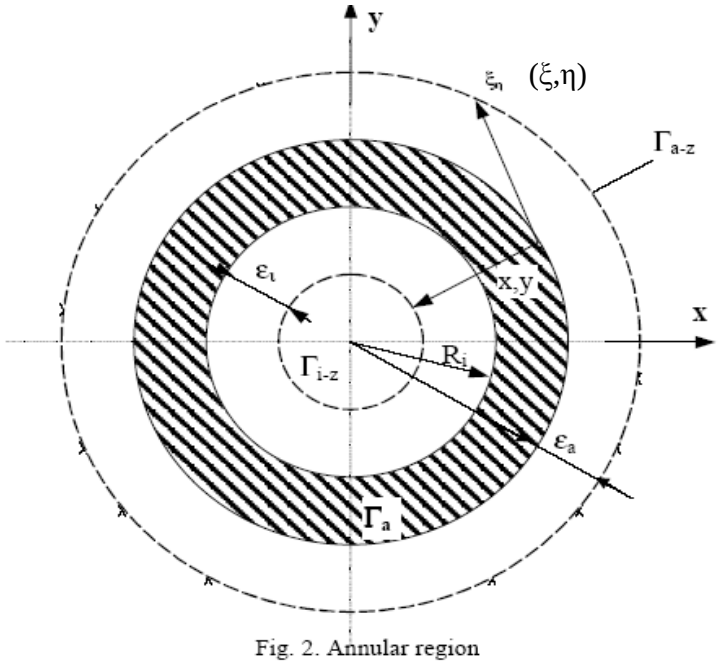

Fig. 2. Annular region

Then approximate solution (6) can be expressed as

$$u(x,y,\varepsilon_i,\varepsilon_a)=\int\limits_{\Gamma_{i-z}} p(\xi,\eta)\cdot ln\left[(x-\xi(\varepsilon_i))^2+(y-\eta(\varepsilon_i))^2\right]ds+$$

$$+\int\limits_{\Gamma_{a-z}} p(\xi,\eta)\cdot ln\left[(x-\xi(\varepsilon_a))^2+(y-\eta(\varepsilon_a))^2\right] \tag{7}$$

On the account of numerical calculation the integral in (7) can be approximated by

– step function and at division arc Γ on N part we have

$$\int\limits_{\Gamma} p(\xi,\eta)\cdot ln\left[(x-\xi)^2+(y-\eta)^2\right]ds=\sum_{i=1}^{N}\int\limits_{\Gamma_{i,i+1}} p(\xi,\eta)\cdot ln\left[(x-\xi)^2+(y-\eta)^2\right]ds=$$

$$=\sum_{i=1}^{N} p_i\cdot ln\left[(x-\xi_i)^2+(y-\eta_i)^2\right]\cdot\Delta s_{i,i+1}=\sum_{i=1}^{N} p_i\cdot\gamma_i(x,y) \tag{8}$$

– piece of linear function with approximation arc $\Gamma_{i,i+1}$ by segment, then

$$\xi=\xi_i+(\xi_{i+1}-\xi_i)\cdot t,\quad \eta=\eta_i+(\eta_{i+1}-\eta_i)\cdot t,\quad p=p_i+(p_{i+1}-p_i)\cdot t$$

$$t\in\langle 0,1\rangle$$

$$\int_{\Gamma} p(\xi,\eta)\cdot ln\left[(x-\xi)^2+(y-\eta)^2\right]ds=\sum_{i+1}^{N}\int_{\Gamma_{i,i+1}} p(\xi,\eta)\cdot ln\left[(x-\xi)^2+(y-\eta)^2\right]ds=$$

$$=\sum_{i+1}^{N}\Delta s_{i,i+1}\left[\, p_i\cdot\int_0^1 ln\left[(x-\xi(t))^2+(y-\eta(t))^2\right]dt+(p_{i+1}-p_i)\int_0^1 t\cdot ln\left[(x-\xi(t))^2+(y-\eta(t))^2\right]dt\right]=$$

$$=\sum_{i=1}^{N+1} p_i\cdot\varphi_i(x,y) \quad (9)$$

– a parabolic function (on an isoparametric plain) with a simultaneous approach of the $\Gamma_{i,i+1,i+2}$, which is a parabola as well

$$\xi=\xi_i\cdot\varphi_1(t)+\xi_{i+1}\cdot\varphi_2(t)+\xi_{i+2}\cdot\varphi_3(t),\quad \varphi_1(t)=2t^2-3t+1$$

$$\eta=\eta_i\cdot\varphi_1(t)+\eta_{i+1}\cdot\varphi_2(t)+\eta_{i+2}\cdot\varphi_3(t),\quad \varphi_2(t)=-4t^2+4t$$

$$p=p_i\cdot\varphi_1(t)+p_{i+1}\cdot\varphi_2(t)+p_{i+2}\cdot\varphi_3(t),\quad p_1(t)=2t^2-t \qquad t\in\langle 0,1\rangle$$

$$\int_{\Gamma} p(\xi,\eta)ln\left[(x-\xi)^2+(y-\eta)^2\right]ds=\sum_{i=1,3,5\ldots}^{N-1}\int_{\Gamma_{i,i+1,i+1}} p(\xi,\eta)\cdot ln\left[(x-\xi)^2+(y-\eta)^2\right]ds=$$

(10)

$$=\sum_{i=1}^{N+1} p_i\cdot\beta_i(x,y)$$

It is worth noticing that if it is assumed that the sources are placed on Γ at points, then

$$p(\xi,\eta) = p_i \cdot \delta(\xi - \xi_i, \eta - \eta_i),\ i = 1,2,\ldots N \text{ and}$$

$$\int_{\Gamma} p(\xi,\eta)\cdot \ln\left[(x-\xi)^2 + (y-\eta)^2\right]\cdot ds = \sum_{i=1}^{N} p_i \cdot \Delta s_{i,i+1} \cdot \ln\left[(x-\xi)^2 + (y-\eta)^2\right] = \sum_{i=1}^{N+1} p_i \cdot \gamma_i(x,y)$$

(11)

The dependence (11) is identical in its structure (8). Depending on approximation of the function p(ξ, η) we obtain:

$$\int_{\Gamma} p(\xi,\eta)\cdot ln\left[(x-\xi)^2 + (y-\eta)^2\right] d\xi = \sum_{i=1}^{N+1} p_i \cdot \alpha_i(x,y) \qquad (12)$$

$$\alpha_i(x,y) = \begin{cases} \varphi_i(x,y) & \text{– the approximation of function } p(\xi,\eta) \text{ by a Dirac function} \\ \beta_i(x,y) & \text{– the approximation of function } p(\xi,\eta) \text{ by linear function} \\ \gamma_i(x,y) & \text{– the approximation of function } p(\xi,\eta) \text{ by isoperimetric parabola} \end{cases}$$

From relationships (8–10) results that functions $\gamma_i(x,y), \varphi_i(x,y), \beta_i(x,y)$ are linear combinations of fundamental solutions.

3. THE SOLUTION TO THE INVERSE PROBLEM

The solution of the equation (3) in a discrete form with consideration of the integration method (9) – (12) is as follows

$$u(x,y,\varepsilon_i,\varepsilon_a)=$$

$$=\int_{\Gamma_{i-z}} p(\xi,\eta)\cdot ln\left[(x-\xi(\varepsilon_i))^2+(y-\eta(\varepsilon_i))^2\right]ds+\int_{\Gamma_{a-z}} p(\xi,\eta)\cdot ln\left[(x-\xi(\varepsilon_a))^2+(y-\eta(\varepsilon_a))^2\right]ds=$$

$$=\sum_{i=1}^{N_{i-z}} p_i\cdot\alpha_i(x,y,\varepsilon_i)+\sum_{i=N_{i-z}+1}^{N_{i-z}+N_{a-z}} p_i\cdot\alpha_i(x,y,\varepsilon_a)=\sum_{i=1}^{N_{i-z}+N_{a-z}} p_i\cdot\alpha_i(x,y,\varepsilon_i,\varepsilon_a) \quad (13)$$

The periodicity of the function of density p on the closed arc Γ, is taken into consideration in the function α_i. For the finite number of nodes $N_{i-z} + N_{a-z}$ the re-creation of the constant function in the area Ω will be taking place with some approximation, so the solution (13) can be developed to:

$$u(x,y,\varepsilon_i,\varepsilon_a)=\sum_{i=1}^{N_{i-z}+N_{a-z}} p_i\cdot\alpha_i(x,y,\varepsilon_i,\varepsilon_a)+p_{N_{i-z}+N_{a-z}+1}=\sum_{i=1}^{N_{i-z}+N_{a-z}+I_{add}} p_i\cdot\alpha_i(x,y,\varepsilon_i,\varepsilon_a)=$$

$$=\{\alpha(x,y,\varepsilon_i,\varepsilon_a)\}^T\{p\} \quad (14)$$

$$\alpha_{N_{i-z}+N_{a-z}+I_{add}}=\begin{cases}0- & \text{then } I_{add}=0 \text{ and the constant in (14) is not considered}\\ 1- & \text{then } I_{add}=1 \text{ and the constant in (14) is considered}\end{cases}$$

Assuming that $M = N_{i\text{-}z} + N_{a\text{-}z} + I_{add}$ the dependency (14) in collocation points $(x_1, y_1),\ldots,(x_{NT}, y_{NT})$ for the condition (4) and in points $(\bar{x}_1, \bar{y}_1),\ldots,(\bar{x}_{Nq}, \bar{y}_{Nq})$ for the condition (5) can be written in a matrix form:

$$\begin{bmatrix} \alpha_1(x_1,y_1) & \cdots & \alpha_M(x_1,y_1) \\ \vdots & & \\ \alpha_1(x_{NT},y_{NT}) & \cdots & \alpha_M(x_{NT},y_{NT}) \\ \dfrac{\partial\alpha_1(\bar{x}_1,\bar{y}_1)}{\partial n} & \cdots & \dfrac{\partial\alpha_M(\bar{x}_1,\bar{y}_1)}{\partial n} \\ \vdots & & \\ \dfrac{\partial\alpha_1(\bar{x}_{Nq},\bar{y}_{Nq})}{\partial n} & \cdots & \dfrac{\partial\alpha_M(\bar{x}_{Nq},\bar{y}_{Nq})}{\partial n} \end{bmatrix} \begin{Bmatrix} p_1 \\ \vdots \\ \\ \vdots \\ \\ \vdots \\ p_M \end{Bmatrix} = \begin{Bmatrix} f(x_1,y_1) \\ \vdots \\ f(x_{NT},y_{NT}) \\ q(\bar{x}_1,\bar{y}_1) \\ \vdots \\ q(\bar{x}_{Nq},\bar{y}_{Nq}) \end{Bmatrix} \tag{15}$$

or in compact matrix form:

$$[\mathrm{A_{inv}}]\{\mathrm{p}\} = \{\mathrm{G}\} \quad \text{hence} \quad \{\mathrm{p}\} = [\mathrm{A_{inv}}]^{\mathrm{I}}\{\mathrm{G}\} \tag{16}$$

$$\dim[\mathrm{A_{inv}}] = (\mathrm{NT} + \mathrm{Nq}) \times \mathrm{M}\,, \quad dim\{p\} = M\,, \quad dim\{G\} = NT + Nq$$

Substituting the equation (16) to (14) we get

$$\mathrm{u}(\mathrm{x},\mathrm{y},\varepsilon_\mathrm{i},\varepsilon_\mathrm{a}) = \{\alpha(\mathrm{x},\mathrm{y},\varepsilon_\mathrm{i},\varepsilon_\mathrm{a})\}^{\mathrm{T}}\{\mathrm{p}\} = \{\alpha(\mathrm{x},\mathrm{y},\varepsilon_\mathrm{i},\varepsilon_\mathrm{a})\}^{\mathrm{T}}[\mathrm{A_{inv}}(\varepsilon_\mathrm{i},\varepsilon_\mathrm{a})]^{\mathrm{I}}\{\mathrm{G}\} \tag{17}$$

so for the vector of disturbed data $\{G + \delta G\}$ disturbed field of temperature is expressed by the dependency

$$\mathrm{u}(\mathrm{x},\mathrm{y},\varepsilon_\mathrm{i},\varepsilon_\mathrm{a}) + \delta\mathrm{u}(\mathrm{x},\mathrm{y},\varepsilon_\mathrm{i},\varepsilon_\mathrm{a}) = \{\alpha(\mathrm{x},\mathrm{y},\varepsilon_\mathrm{i},\varepsilon_\mathrm{a})\}^{\mathrm{T}}[\mathrm{A_{inv}}(\varepsilon_\mathrm{i},\varepsilon_\mathrm{a})]^{\mathrm{I}}\{\mathrm{G} + \delta\mathrm{G}\} \tag{18}$$

By subtracting Eq. (18) from Eq. (17), we obtain the value of perturbation δu namely

$$\delta\mathrm{u}(\mathrm{x},\mathrm{y},\varepsilon_\mathrm{i},\varepsilon_\mathrm{a}) = \{\alpha(\mathrm{x},\mathrm{y},\varepsilon_\mathrm{i},\varepsilon_\mathrm{a})\}^{\mathrm{T}}[\mathrm{A_{inv}}(\varepsilon_\mathrm{i},\varepsilon_\mathrm{a})]^{\mathrm{I}}\{\delta\mathrm{G}\} \tag{19}$$

The solution of the system of equation (16) with ill conditioned matrix [A_{inv}] can be obtained by means of Tichonov regularization, which leads to the minimization of a functional

$$J(\{p\}) = \left\| [A_{inv}(\varepsilon_i, \varepsilon_a)]\{p\} - \{G\} \right\|^2 + \alpha \cdot \left\| \{p\} - \{p_0\} \right\|^2, \quad \alpha > 0 \qquad (20)$$

where vector $\{p_0\}$ is an unknown solution of equation. Minimization of functional (20) leads to a solution of system of equation

$$\begin{bmatrix} [A_{inv}(\varepsilon_i, \varepsilon_a)] \\ \alpha \cdot I \end{bmatrix} \begin{Bmatrix} p_1 \\ \vdots \\ p_M \end{Bmatrix} = \begin{Bmatrix} \{G\} \\ \alpha \cdot \{p_0\} \end{Bmatrix} \qquad (21)$$

in a least squares sense. The equation (21) can be written in a symbolic form

$$[A_{inv,\alpha}(\varepsilon_i, \varepsilon_a)]\{p\} = \begin{Bmatrix} \{G\} \\ \alpha\{p_0\} \end{Bmatrix} \quad \text{or} \quad \{p\} = [A_{inv,\alpha}(\varepsilon_i, \varepsilon_a)]^I \begin{Bmatrix} \{G\} \\ \alpha\{p_0\} \end{Bmatrix} \qquad (22)$$

$$\dim[A_{inv,\alpha}(\varepsilon_i, \varepsilon_a)] = (NT + Nq + M) \cdot M, \quad \dim\{\{G\}, \alpha\{p_0\}\} = NT + Nq + M$$

Because the vector $\{p_0\}$ is unknown, then it can be determined with iteration algorithm

$$\{p_{n+1}\} = [A_{inv,\alpha}(\varepsilon_i, \varepsilon_a)]^I \begin{Bmatrix} \{G\} \\ \alpha\{p_n\} \end{Bmatrix}, \quad n = 0,1,2,\ldots \qquad (23)$$

By decomposing matrix $[A_{invr,\alpha}(\varepsilon_i,\varepsilon_a)]^I$ into two matrices [AI] i [BI] in the following way

$$[A_{inv,\alpha}(\varepsilon_i, \varepsilon_a)]^I \begin{Bmatrix} \{G\} \\ \alpha\{p_n\} \end{Bmatrix} = [AI]\{G\} + [BI] \cdot \{p_n\}$$

we get:

$$\{p_{n+1}\} = [AI]\{G\} + [BI] \cdot \{p_n\} = [AI] \cdot \left([BI]^0 + [BI]^1 + [BI]^2 + \ldots + [BI]^n \right) + [BI]^{n+1} \cdot \{p_0\}$$

If $\|[BI]\| < 1$ then the series is convergent for $\alpha > 0$ and any initial vector $\{p_0\}$.

4. NUMERICAL CALCULATIONS

For the testing purposes of the numerical properties of the proposed method let's consider an exact solution $u(x,y)$ fulfilling the following conditions:

– on the outside boundary of the ring

$$u\big|_{r=R_a} = T_a \tag{24}$$

– on the inner boundary of the ring

$$u\big|_{r=R_i} = \frac{1}{2}(T_i + T_a) + \left[\frac{1}{2}(T_a - T_i) - \gamma\right] \cdot \cos\varphi, \quad \varphi \in \langle 0, 2\pi \rangle, \quad T_i < T_a \tag{25}$$

For $\gamma = 0$ and $T_a > T_i$ the heat flows inwards the ring.

The solution of equation $\Delta u = 0$ with boundary conditions (24) and (25) has a form

$$u(r,\varphi) = T_a \cdot \frac{\ln\frac{r}{R_i}}{\ln\frac{R_a}{R_i}} + \frac{T_i + T_a}{2} \cdot \frac{\ln\frac{R_a}{r}}{\ln\frac{R_a}{R_i}} - \left(\frac{T_a - T_i}{2} - \gamma\right) \cdot \frac{R_i}{R_a^2 - R_i^2} \cdot \left(r - \frac{R_a^2}{r}\right) \cdot \cos\varphi \tag{26}$$

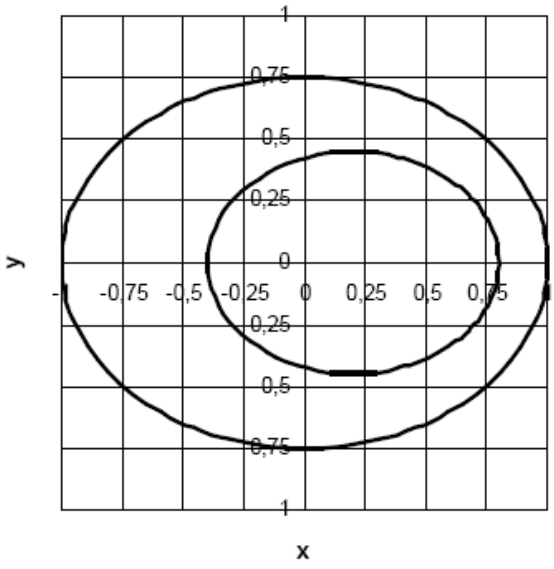

Fig. 3. Calculation area

ENTROPY FUNCTIONALS

For finding the optimal values of parameters ε_i and ε_a we minimize the functional of intensity of entropy production or dissipation energy

$$\sigma = \int_{\Gamma_{i-z} \cup \Gamma_{a-z}} \frac{1}{T} \frac{\partial T}{\partial n} \, ds \quad , \quad \Psi = \int_{\Gamma_{i-z} \cup \Gamma_{a-z}} \ln T \, \frac{\partial T}{\partial n} \, ds \tag{29}$$

Introducing the dimensionless temperature u

$$T = T_0 \cdot (1 + u), \quad 0 < T/T_0 \le 1, \quad T_0 \text{ –reference temperature}$$

then the intensity of entropy production takes the form for $\Delta u = 0$

$$\sigma = -\int_\Gamma \frac{\frac{\partial u}{\partial n}}{1+u} ds = -\int_\Gamma \frac{\partial}{\partial n} \ln(1+u) ds = -\int_\Omega \operatorname{div}(\nabla \ln(1+u)) d\Omega = -\int_\Omega \left(-\frac{1}{(1+u)^2} \cdot (\nabla u)^2 + \frac{1}{1+u} \cdot \Delta u \right) d\Omega =$$

$$= \int_\Omega \frac{1}{(1+u)^2} \cdot (\nabla u)^2 \, d\Omega \le A_1 \cdot \int_\Omega (\nabla u)^2 \, d\Omega = A_1 \cdot \Theta, \quad \Theta = \int_\Omega (\nabla u)^2 \, d\Omega \tag{a}$$

$$A_1 = \max \frac{1}{(1+u)^2}$$

or as a quadratic functional

$$\sigma = \int_\Omega \frac{1}{(1+u)^2} \cdot (\nabla u)^2 d\Omega = \int_\Omega (\nabla \ln(1+u))^2 d\Omega = \int_\Omega (\nabla w)^2 d\Omega, \quad w = \ln(1+u)$$

Energy dissipation functional

$$\psi = \int_\Gamma \ln(1+u) \frac{\partial u}{\partial n} ds = \int_\Gamma \frac{\partial}{\partial n} [(1+u)(\ln(1+u) - 1)] ds = \int_\Gamma \frac{\partial}{\partial n} [(1+u)\ln(1+u)] ds =$$

$$= \int_\Omega \operatorname{div}(\nabla((1+u)\ln(1+u))) \cdot d\Omega = \int_\Omega \left(\frac{1}{1+u} \cdot (\nabla u)^2 + (\ln(1+u) + 1) \cdot \Delta u \right) d\Omega =$$

$$= \int_{\Omega} \frac{1}{1+u} (\nabla u)^2 \, d\Omega \le A_2 \int_{\Omega} (\nabla u)^2 \, d\Omega = A_1 \cdot \Theta \qquad \text{(b)}$$

$$A_2 = \max \frac{1}{1+u}, \quad u > 0$$

or as quadratic functional

$$\psi = \int_{\Omega} \frac{1}{1+u} \cdot (\nabla u)^2 \, d\Omega = \int_{\Omega} \left(\nabla 2 \cdot \sqrt{1+u}\right)^2 d\Omega = \int_{\Omega} (\nabla p)^2 \, d\Omega, \quad p = 2\sqrt{1+u}$$

For u>0 holds $(1 + u)^2 > 1 + u > 0$, hence

$$\sigma = \int_{\Omega} \frac{1}{(1+u)^2} \cdot (\nabla u)^2 \, d\Omega < \int_{\Omega} \frac{1}{1+u} \cdot (\nabla u)^2 \, d\Omega = \psi < \int_{\Omega} (\nabla u)^2 \, d\Omega \quad \text{or}$$

$$\sigma < \psi < \Theta$$

$\sigma = \psi$ = Θ only for u = const, then $\nabla u = 0$.

For $|u| < 1$ the following expansion into series holds

$$\frac{1}{1+u} = 1 - u + u^2 - u^3 + \ldots \quad \text{or} \quad \ln(1+u) = u - \frac{1}{2}u^2 + \frac{1}{3}u^3 - \frac{1}{4}u^4 + \ldots$$

and neglecting the terms u^2, u^3…,

$$\sigma = -\int_{\Gamma} \frac{\frac{\partial u}{\partial n}}{1+u} ds = -\int_{\Gamma} \left(1 - u + u^2 - u^3 + \ldots\right) \frac{\partial u}{\partial n} ds = -\int_{\Gamma} \frac{\partial u}{\partial n} ds + \int_{\Gamma} u \frac{\partial u}{\partial n} ds - \ldots = \int_{\Gamma} u \frac{\partial u}{\partial n} ds - \ldots$$

$$\psi = \int_{\Gamma} \ln(1+u) \frac{\partial u}{\partial n} ds = \int_{\Gamma} \left(u - \frac{1}{2}u^2 + \frac{1}{3}u^3 - \frac{1}{4}u^4 + \ldots\right) \frac{\partial u}{\partial n} ds = \int_{\Gamma} u \frac{\partial u}{\partial n} ds - \ldots$$

For small values of $|u|$, σ and ψ can be relaced by functional ζ

$$\zeta = \int_{\Gamma} u \frac{\partial u}{\partial n} ds \qquad \text{(c)}$$

On the basis of Schwarz-Buniakowsky inequality

$$\sigma^2=\left(-\int_\Gamma \frac{\frac{\partial u}{\partial n}}{1+u}ds\right)^2 \le \int_\Gamma \frac{1}{(1+u)^2}\cdot\int_\Gamma\left(\frac{\partial u}{\partial n}\right)^2 ds=c_1\cdot\int_\Gamma\left(\frac{\partial u}{\partial n}\right)^2 ds=c_1\cdot\chi,\quad \chi=\int_\Gamma\left(\frac{\partial u}{\partial n}\right)^2 ds$$

$$\psi^2=\left(-\int_\Gamma \ln(1+u)\frac{\partial u}{\partial n}ds\right)^2 \le \int_\Gamma(\ln(1+u))^2\cdot ds\cdot\int_\Gamma\left(\frac{\partial u}{\partial n}\right)^2 ds=c_2\int_\Gamma\left(\frac{\partial u}{\partial n}\right)^2=c_2\cdot\chi$$

$$\zeta^2=\left(\int_\Gamma u\frac{\partial u}{\partial n}ds\right)^2 \le \int_\Gamma u^2 ds\cdot\int_\Gamma\left(\frac{\partial u}{\partial n}\right)^2 ds=c_3\cdot\int_\Gamma\left(\frac{\partial u}{\partial n}\right)^2=c_3\cdot\chi$$

$$\chi=\int_\Gamma\left(\frac{\partial u}{\partial n}\right)^2 ds=\int_\Gamma q^2 ds,\quad q=\frac{\partial u}{\partial n} \tag{d}$$

Functionals σ, ψ, ζ, I, χ are results of second law of the thermodynamic.

Functionals for damping of oscillation at the boundary:

– functional with first derivative of temperature, along the boundary

$$T_s=\int_\Gamma\left(\frac{\partial T/T_0}{\partial s}\right)^2 ds=\int_\Gamma\left(\frac{\partial u}{\partial s}\right)^2\cdot ds \tag{e}$$

– functional with first derivative of heat flux, along the boundary

$$T_{ns}=\int_\Gamma\left(\frac{\partial}{\partial s}\frac{\partial T/T_0}{\partial n}\right)^2 ds=\int_\Gamma\left(\frac{\partial q}{\partial s}\right)^2 ds \tag{f}$$

– functional with second derivative of temperature, along the boundary

$$T_{ss}=\int_\Gamma\left(\frac{\partial}{\partial s}\frac{\partial T/T_0}{\partial s}\right)^2 ds=\int_\Gamma\left(\frac{\partial^2 T/T_0}{\partial s^2}\right)^2 ds=\int_\Gamma\left(\frac{\partial u^2}{\partial s^2}\right)^2 ds \tag{g}$$

Minimization of functionals σ, ψ, ζ, χ, T_s, T_{ns}, T_{ss} due to parameter ε_i i ε_a delivere the stavile solution of Cauchy problem.

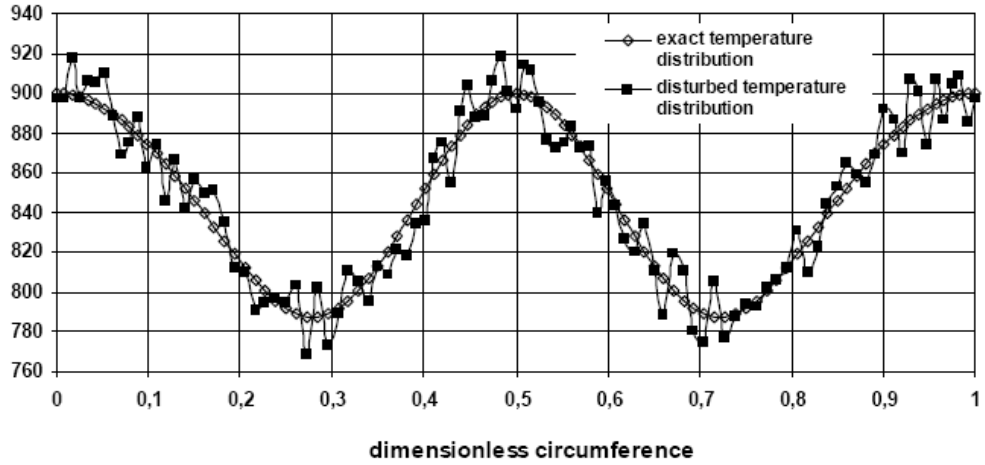

Fig. 4. Given temperature distribution on the boundary Γ_a.

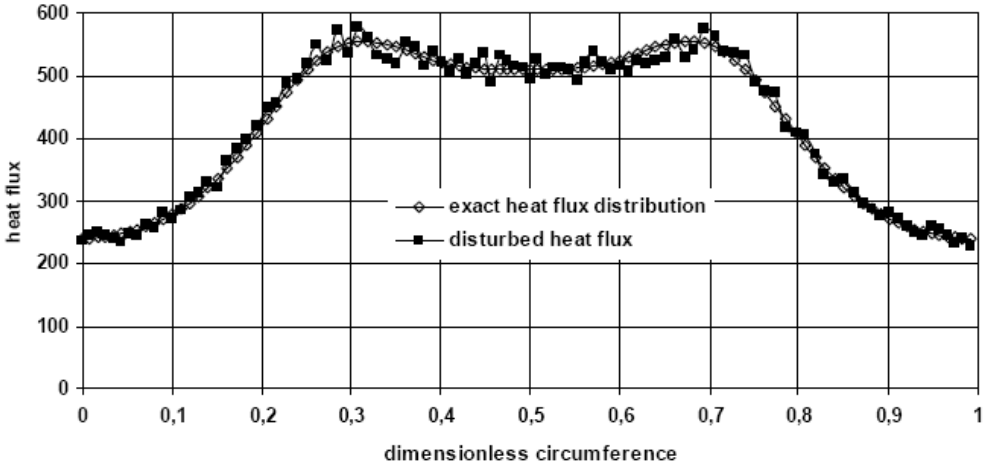

Fig. 5. Given heat flux distribution on the boundary Γ_a.

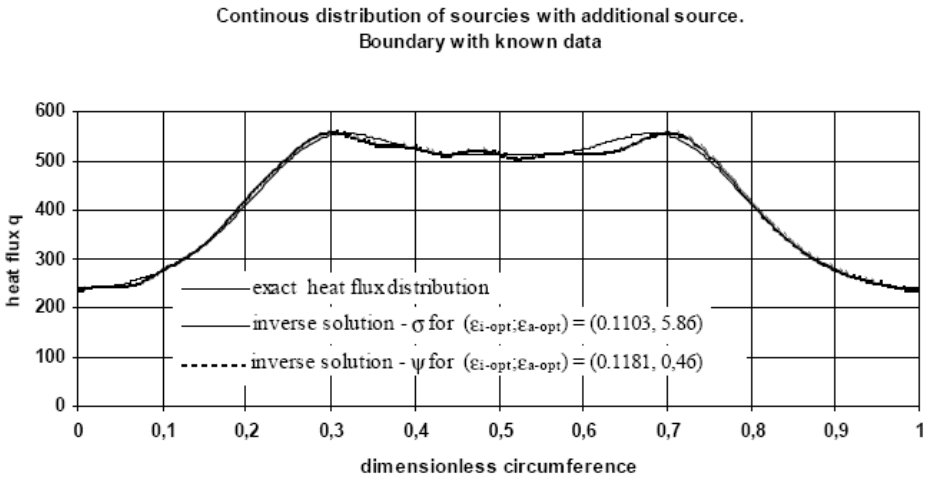

Fig. 6. Comparing between the exact and calculated heat flux from the solution of inverse problem. Outer boundary Γ_a

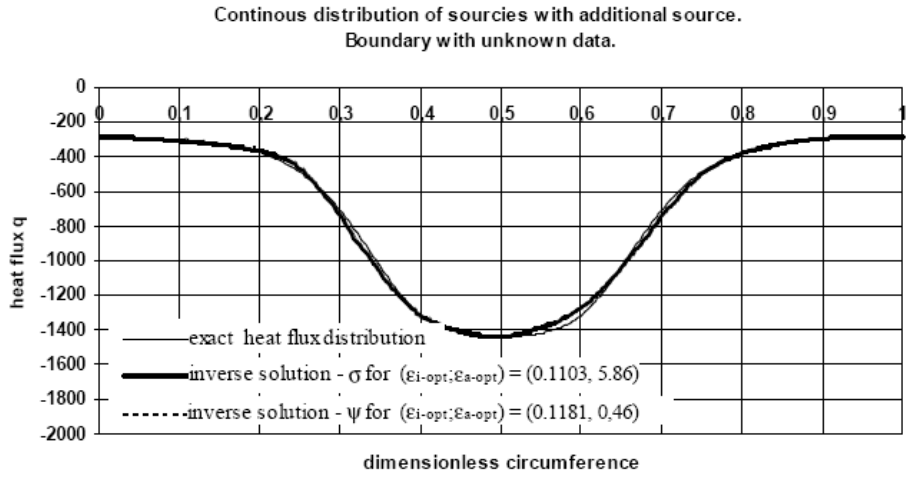

Fig. 7. Comparing between the exact and calculated heat flux from the solution of in verse problem. Inner boundary Γ_i.

5. FINAL REMARKS

- The discussed method of fundamental solution applied to solve the inverse problem is based on the search of the power of sources on the removed boundary in relation to the boundary of the given region.

- The introduction of the removed boundary allows to avoid the integration of the singular functions which makes the numerical calculations much faster and easier.

- The distance of removal of the boundaries ε_a and ε_i from the boundaries Γ_a and Γ_i worsens the conditions of the matrix of the inverse problem. As the result the choice of the parameters of the boundary removal ε_i and ε_a in order to obtain the best solutions with regard to the selected criterions remains crucial.

- The problem discussed in this paper is in fact a Cauchy problem for the Laplace equation and is particularly sensitive to the errors in data.

- The influence of the disturbances is presented in graphs 6 and 7.

A NEW ALGORITHM OF SOLVING INVERSE PROBLEMS OF HEAT CONDUCTION

1. Formulation of Cauchy problem for a multiply connected region

Let us consider stationary heat flow in a multiply connected region Ω confined with the boundary Γ (Fig.1).

$$\Delta T = 0, \tag{1}$$

$$\Gamma = \Gamma_{out} \cup \Gamma_{in}, \qquad \Gamma_{in} = \bigcup_{k=1}^{n} \Gamma_{ink} . \tag{2}$$

Knowing the heat flux and temperature values at the boundary Γ_{out}

$$T\Big|_{\Gamma_{out}} = T_{out}, \quad \left.\frac{\partial T}{\partial n}\right|_{\Gamma_{out}} = q_{out}, \tag{3}$$

one should find out the distribution of heat fluxes and temperatures at the inner boundaries Γ_{in}.

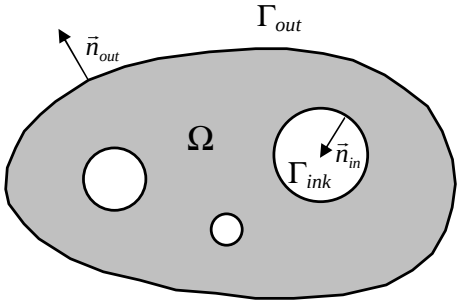

Fig.1.

The problem is to be solved iteratively by defining a direct problem for the region in the following way:

$$\left.\frac{\partial T}{\partial n}\right|_{\Gamma_{out}} = q_{out}, \qquad \left.\frac{\partial T}{\partial n}\right|_{\Gamma_{in}} = g . \tag{4}$$

Normal derivative at the Γ_i boundary is iteratively modified so as to achieve minimal value of the functional

$$J[g] = \frac{1}{2} \int_{\Gamma_{out}} (T[g] - T_{out})^2 \, ds \tag{5}$$

3. Solution of the inverse problem

Taking into account arbitrary shape of the Ω region the equation (1) is solved with Finite Element Method. Multiplication of the Laplace equation by the test function φ, integration at the Ω region, and application of the Ostrogradski-Gauss theorem provide:

$$\int_{\Omega} \Delta T \cdot \varphi \cdot dx = -\int_{\Omega} \nabla T \cdot \nabla \varphi \cdot dx + \int_{\Gamma_{out}} \frac{\partial T}{\partial n} \cdot \varphi \cdot ds + \int_{\Gamma_{in}} \frac{\partial T}{\partial n} \cdot \varphi \cdot ds = 0 . \tag{6}$$

Consideration of (4) gives

$$\int_{\Omega} \nabla T \cdot \nabla \varphi \cdot dx = \int_{\Gamma_{out}} q_{out} \cdot \varphi \cdot ds + \int_{\Gamma_{in}} g \cdot \varphi \cdot ds . \tag{7}$$

Since the condition at the Γ_{in} boundary is subject to changes, solution of the Laplace equation is affected accordingly. Let us calculate the first variation of the functional:

$$\delta T = u = \lim_{\lambda \to 0} \frac{T(g + \lambda \delta g) - T(g)}{\lambda}, \tag{8}$$

Formulation of the equation (4) for $g+\lambda\delta g$ and g

$$\int_{\Omega} \nabla T(g + \lambda \delta g) \cdot \nabla \varphi \cdot dx = \int_{\Gamma_{out}} q_{out} \cdot \varphi \cdot ds + \int_{\Gamma_{in}} (g + \lambda \delta g) \cdot \varphi \cdot ds , \tag{9}$$

$$\int_{\Omega} \nabla T(g) \cdot \nabla \varphi \cdot dx = \int_{\Gamma_{out}} q_{out} \cdot \varphi \cdot ds + \int_{\Gamma_{in}} g \cdot \varphi \cdot ds , \tag{10}$$

its subtraction by sides and division by λ allows for calculating the limit for $\lambda \to 0$ which gives:

$$\int_{\Omega} \nabla u \cdot \nabla \varphi \cdot dx = \int_{\Gamma_{in}} \delta g \cdot \varphi \cdot ds . \tag{11}$$

Similar procedure for the functional $J[g]$ provides:

$$\begin{aligned} &\lim_{\lambda \to 0} \frac{J(g + \lambda \delta g) - J(g)}{\lambda} = \lim_{\lambda \to 0} \frac{1}{2\lambda} \left[\int_{\Gamma_{out}} (T(g + \lambda \delta g) - T_{out})^2 ds - \int_{\Gamma_{out}} (T(g) - T_{out})^2 ds \right] = \\ &= \lim_{\lambda \to 0} \left[\int_{\Gamma_{out}} \frac{T(g + \lambda \delta g) - T(g)}{\lambda} \frac{(T(g + \lambda \delta g) + T(g) - 2T_{out})}{2} ds \right] = \int_{\Gamma_{out}} u \cdot (T(g) - T_{out}) \cdot ds \end{aligned} , \tag{12}$$

$$\frac{\partial J}{\partial \lambda} = \int_{\Gamma_{out}} (T(g) - T_{out}) \cdot u \cdot ds . \tag{13}$$

Since we search the changes of heat flux δg at the inner boundary, the boundary integral Γ_{out} should be transformed into the boundary integral Γ_{in}. Hence, let us formulate the following equation for this purpose

$$\int_{\Omega} \nabla \psi \cdot \nabla p \cdot dx = \int_{\Gamma_{out}} (T - T_{out}) \cdot \psi \cdot ds , \qquad \left. \frac{\partial p}{\partial n} \right|_{\Gamma_{out}} = T - T_{out} , \qquad \left. \frac{\partial p}{\partial n} \right|_{\Gamma_{in}} = 0 . \tag{14}$$

Substitution of p into φ in equation (11) and u into ψ in (14) (this may be done as φ and ψ are base functions, while p and u are expressed by linear combinations of the base functions) gives the following equation:

$$\int_{\Gamma_{in}} \delta g \cdot \varphi \cdot ds = \int_{\Gamma_{out}} \left(T(g) - T_{out}\right) \cdot u \cdot ds \,. \tag{15}$$

The above consideration enables formulating an algorithm of the inverse problem solution. Knowledge of the flux distribution g^n in the n-th iteration at the Γ_{in} boundary allows for finding the T^n solution of the equation

$$\int_{\Omega} \nabla T^n \cdot \nabla \varphi \cdot dx = \int_{\Gamma_{out}} q_{out} \cdot \varphi \cdot ds + \int_{\Gamma_{in}} g^n \cdot \varphi \cdot ds \,. \tag{16}$$

The equation

$$\int_{\Omega} \nabla \psi \cdot \nabla p^n \cdot dx = \int_{\Gamma_{out}} \left(T^n - T_{out}\right) \cdot \psi \cdot ds \tag{17}$$

serves for finding the p^n function. A new approximation g^n of the flux distribution at the Γ_{in} boundary is obtained from the formula

$$g^{n+1} = g^n - \eta p^n \,, \tag{18}$$

where $\eta \in (0,1)$. The interation is terminated when the condition

$$\left|T^{n+1} - T^n\right| < \varepsilon \,. \tag{19}$$

is met. Value of the parameter η may be optimally chosen in every iteration step. The solution in the n+1 iteration step depends on the parameter η, taking the following form:

$$\int_{\Omega} \nabla T_{\eta}^{n+1} \cdot \nabla \varphi \cdot dx = \int_{\Gamma_{out}} q_{out} \cdot \varphi \cdot ds + \int_{\Gamma_{in}} g^{n+1} \cdot \varphi \cdot ds \,. \tag{20}$$

In the next step of iteration the solution is sought in the following form:

$$T_{\eta}^{n+1} = T^n - \eta u\left(p^n\right), \tag{21}$$

thus allowing for finding the function u:

$$\int_{\Omega} \nabla u\left(p^n\right) \cdot \nabla \varphi \cdot dx = \int_{\Gamma_{in}} p^n \cdot \varphi \cdot ds \,. \tag{22}$$

Once the functional is calculated for the next iteration

$$\begin{aligned} J\left[g^{n+1}\right] = J\left[g^n - \eta p^n\right] &= \frac{1}{2} \int_{\Gamma_{out}} \left(T^n - \eta u\left(p^n\right) - T_{out}\right)^2 ds = \\ &= \frac{1}{2} \int_{\Gamma_{out}} \left(T^n - T_{out}\right)^2 ds - \eta \int_{\Gamma_{out}} \left(T^n - T_{out}\right) u\left(p^n\right) ds + \frac{1}{2} \eta^2 \int_{\Gamma_{out}} u^2\left(p^n\right) ds \end{aligned} \,, \tag{23}$$

it becomes evident that the problem converts itself into calculation of extreme point of the quadratic equation:

$$a\eta^2 + b\eta + c = 0 \,, \tag{24}$$

where

$$a = \frac{1}{2}\int_{\Gamma_a} u^2\left(p^n\right)ds\,, \qquad b = -\int_{\Gamma_a}\left(T^n - T_{out}\right)u\left(p^n\right)ds\,, \qquad c = \frac{1}{2}\int_{\Gamma_a}\left(T^n - T_{out}\right)^2 ds\,. \tag{25}$$

Finally, the optimal value of the parameter η is given by the formula:

$$\eta_{opt} = \frac{\int_{\Gamma_a}\left(T^n - T_{out}\right)u\left(p^n\right)ds}{\int_{\Gamma_a} u^2\left(p^n\right)ds}\,. \tag{26}$$

4. Numerical calculation

The above described algorithm has been used for solving an inverse problem for a ring of the radius r_0=0.5 (Fig. 2) with the help of the Felics program. It is a file of numerical procedures designed for solving differential equations with Finite Element Method. The program has been developed in the Institute of Mathematics of the Munich University of Technology.

The ring region was divided into 11348 triangle elements. In order to approximate the heat flux density the outer boundary of the ring was divided into 312 ranges, while the inner boundary into 156 ranges.

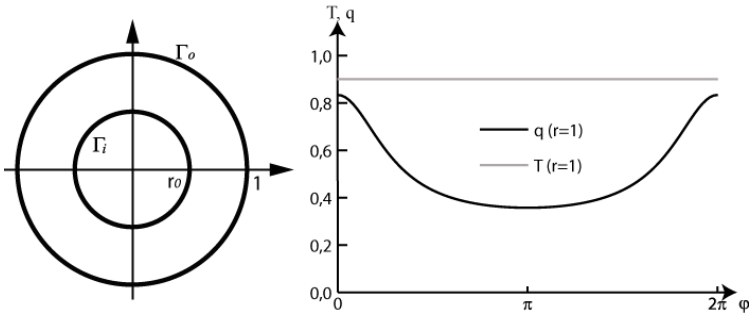

Fig. 2. Temperature and heat flux density distributions at the outer boundary of the ring

Temperature and heat flux density patterns at the outer boundary of the ring (Fig. 2) have been determined from the analytical solution [8]:

$$T(r,\varphi) = T_c + C \cdot \ln r + C \cdot \sum_{m=1}^{\infty} \frac{1}{2m} \left[(ar)^m - \left(\frac{a}{r}\right)^m \right] \cos(m\varphi). \tag{27}$$

Temperature distributions at the inner boundary of the ring for the analytical and numerical solutions are shown in Fig. 3.

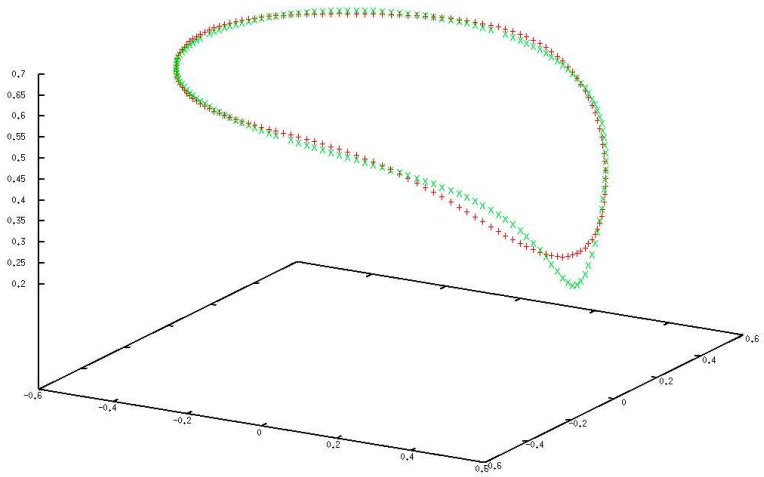

Fig. 3. Comparison of temperatures at the inner boundary of the ring obtained from analytical (green) and numerical (red) solutions

5. Summary

The results presented in Fig. 3 show that the functional [6] more quickly converges to the minimum (the final value of the functional [6] was of the order of 10^{-4}) than the temperature at the inner boundary of the ring to the accurate solution. Hence, it can be admitted that it is a sign of ill-conditioning of the inverse problem. What is more important, the solution obtained this way is not subject to oscillations as in the paper [5], where the oscillation had to be damped with the SVD algorithm.

Modification of the presented algorithm should be additionally analyzed, with a view to reduce the difference shown in Fig. 3.

The solution presented here may be considered as an example formulation of the problem. The aim of the present paper was to test the new algorithm of inverse problems. In the next stage the test of a modified algorithm should be made, with consideration of mean-square fulfilling of the conditions (3).

The work has been carried out within the framework of the Ministry of Science and Education Grant No. 3134/B/T02/2007/33

SOLUTION OF CAUCHY PROBLEM TO STATIONARY HEAT CONDUCTION EQUATION BY MODYFIED METHOD OF ELEMENTARY BALANCES WITH INTERPOLATION OF THE SOLUTION IN PHYSICAL PLANE

1. Formulation of a modified method of elementary balances (MCVM – Modified Control Volume Method)

In the modified method of elementary balances the domain Ω is divided into sub-domains Ω_n. The unknown solution of the differential equation is interpolated in every element of the domain with the help of base functions

$$T(P)=\sum_{i=1}^{m} T_i \cdot \varphi_i(P). \tag{1}$$

The base functions φ_i are determined as follows

$$\varphi_i(P_j)=\begin{cases} 1 & for \quad i=j \\ 0 & for \quad i\neq j \end{cases}, \tag{2}$$

where the points P_j are interpolation nodes belonging to the Ω_n sub-domain. In the case of four nodes of a quadrilateral element or six nodes of a triangular one (Fig. 1) the base function φ_i is a product of two linear functions [20]

$$\varphi_i(x,y)=\prod_{j=(j_1,j_2)} \frac{A_j x+B_j y+C_j}{A_j x_i+B_j y_i+C_j}, \tag{3}$$

where j_1, j_2 are the numbers of lines connecting the mesh nodes of the element (Table 1), $A_j x+B_j y+C_j = 0$ being equation of the j-th straight line. More general formulation of the interpolation function of such a form in the mesh element is provided by [20]. An important property of the base functions (3) lies in their zeroing at the sides opposite to the P_i node that in consequence leads to the disappearance of some integrals in the calculation process.

The control surface $\partial\Sigma$, on which the energy is balanced, is created around each of the mesh nodes. Figure 2 shows the way of generating the control surface (broken line) for 4-node and 9-node elements of a quadrilateral mesh.

For six-node element of a triangular mesh the shape of the control surface (Fig. 3a) becomes more complicated, since in this case the control surface coincides with the mesh lines. This leads to overlapping of control surfaces around various points (Fig. 3b).

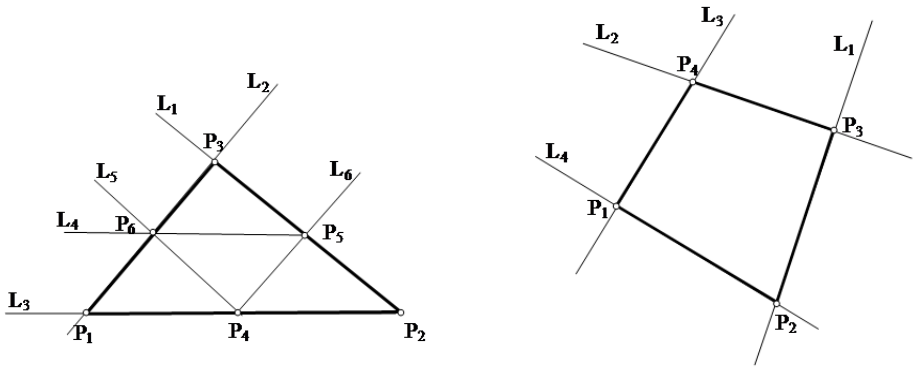

Figure 1: Arrangement of 6 mesh nodes of a triangular element or 4 nodes in a quadrilateral one

Table 1: The numbers j_1, j_2 of the straight line for the i-th base function

i	Triangle		tetragon	
	j_1	j_2	j_1	j_2
1	1	5	1	2
2	2	6	2	3
3	3	4	3	4
4	1	2	4	1
5	2	3		
6	3	1		

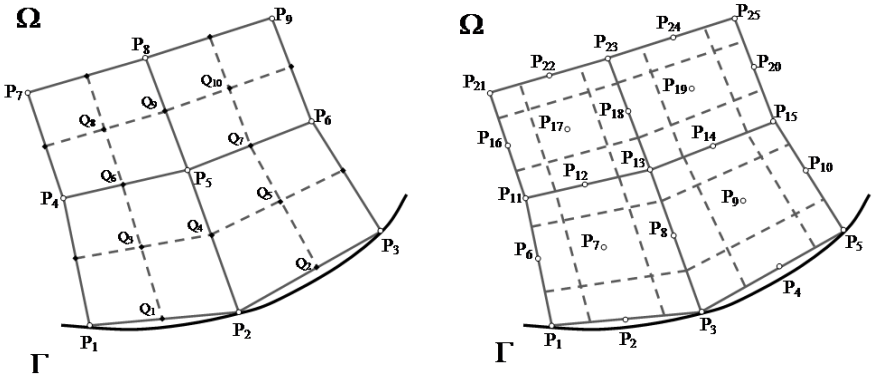

Figure 2: Four-node and nine-node elements of a quadrilateral mesh. The solid line denotes an interpolation mesh while the broken one is for the balance mesh.

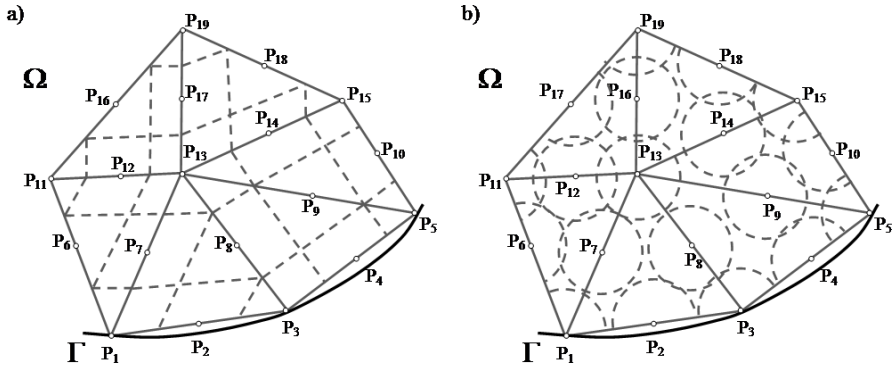

Figure 3: Six-node element of a triangular mesh. An example of control surface formulation (broken line) – a) polygonal region of balancing around node, b) circular region of balancing.

For the point $P_5 \in \Omega$ (Fig. 2) the open polygon $Q_3Q_4Q_5Q_7Q_9Q_{10}Q_8Q_6Q_3$, is a control surface $\partial\Sigma_5$, while for the point $P_2 \in \Gamma$ – it is the open polygon $P_2Q_1Q_3Q_4Q_5Q_2P_2$. In the case of a six-node element of a triangular mesh the situation is more complex. Four cases are possible:

- $P_{13} \in \Omega$ - the control surface is defined by the open polygon $P_1\ P_3\ P_5\ P_{15}\ P_{19}\ P_{11}\ P_1$,
- $P_8 \in \Omega$ - the control surface is defined by the open polygon $P_1\ P_3\ P_5\ P_{13}\ P_1$,
- $P_3 \in \Gamma$ - the control surface is defined by the open polygon $P_3\ P_5\ P_{13}\ P_1\ P_3$,
- $P_2 \in \Gamma$ - the control surface is defined by the open polygon $P_1\ P_3\ P_{13}\ P_1$.

The example shows that the control surfaces built on a triangular mesh are not disjoint.

Energy balance on the control surface for stationary heat conduction equation $div(\nabla T)=0$ performed with the use of the Gauss-Ostrogradski theorem around each point $P_i \in \Omega$ leads to the relationship

$$\int_{\Sigma_i} div(\lambda \nabla T)\, d\Sigma = \oint_{\partial\Sigma_i} \lambda \frac{\partial T}{\partial n} ds = 0\,, \tag{4}$$

while for the point $P_i \in \Gamma$

$$\int_{\partial\Sigma_i} \lambda \frac{\partial T}{\partial n} ds + \int_{\Gamma_i} q ds = 0\,, \tag{5}$$

where $\partial\Sigma_i$ is a control surface around the i-th mesh point, Γ_i is a part of the outer boundary that coincides with the control surface around the i-th point.

Taking into account that the Kirchhoff substitution

$$\vartheta = \int_0^T \lambda(u)\, du$$

transforms the non-linear equation $div(\nabla T)=0$ into linear one $\Delta\vartheta = 0$, we assume $\lambda=1$ for further consideration.

For the point $P_5 \in \Omega$ (Fig. 2) the energy balance is as follows:

$$\oint_{\partial\Sigma_i} \frac{\partial T}{\partial n} ds = \int_{Q_6Q_3Q_4} \frac{\partial T}{\partial n} ds + \int_{Q_4Q_5Q_7} \frac{\partial T}{\partial n} ds + \int_{Q_7Q_{10}Q_9} \frac{\partial T}{\partial n} ds + \int_{Q_9Q_8Q_6} \frac{\partial T}{\partial n} ds = 0\,, \tag{6}$$

while in case of $P_2 \in \Gamma$

$$\int_{\partial\Sigma_i} \frac{\partial T}{\partial n} ds + \int_{\Gamma_i} \frac{\partial T}{\partial n} ds = \int_{Q_1 Q_3 Q_4} \frac{\partial T}{\partial n} ds + \int_{Q_4 Q_5 Q_2} \frac{\partial T}{\partial n} ds + \int_{P_2 Q_1} q ds + \int_{Q_2 P_2} q ds = 0 . \tag{7}$$

Density of the heat flux q between the points of the Γ boundary is approximated with the help of a linear function

$$\int_{P_2 Q_1} q ds + \int_{Q_2 P_2} q ds = |P_2 Q_1| \frac{(q(Q_1) + q(P_2))}{2} + |P_2 Q_2| \frac{(q(Q_2) + q(P_2))}{2} .$$

The substitution the integrals calculated in the manner, into the equations (6) and (7) provides an equation including unknown values of the $T(x,y)$ function in the mesh nodes and the heat flux values at the Γ boundary. The upper index of the base function φ is the number of the mesh element.

The similar procedure is applied in the case of the triangular mesh. The energy balance around each of the nodes provides the system of equations

$$\begin{aligned} A_{\alpha\beta} \cdot T_\alpha + A_{\beta\beta} \cdot T_\beta &= 0 \\ A_{\alpha\alpha} \cdot T_\alpha + A_{\alpha\beta} \cdot T_\beta &= B_\alpha \cdot Q_\alpha \end{aligned} . \tag{8}$$

Each of the equations of the system (8) is related to energy balance around the mesh node. The points are located on inside the Ω domain (the vector T – index β) or at the Γ boundary (the vectors T, Q – with indexes α). Denote the numbers of outer and inner mesh nodes as n_α, n_β, the number of equations with unknown T_α, Q_α, T_β. It amounts to $(2n_\alpha+n_\beta)$ of unknowns. Missing T_α, Q_α values are determined from boundary conditions.

The system of equations (8) allows for eliminating the T_β vector

$$T_\beta = -A_{\beta\beta}^{-1} A_{\beta\alpha} T_\alpha , \tag{9}$$

that provides the relationship between temperature and the heat flux at the domain boundary known from the Boundary Element Method

$$A T_\alpha = B Q_\alpha . \tag{10}$$

Recapitulating, one can state that in the classical method the balancing is based on consistency of the fluxes between the control domains. In a general case considered here the balance occurs in mesh around the node, while the control domains may contain each other. Therefore, the present approach to the method of elementary balances is distinguished by the following characteristic features:

a) in every mesh element the temperature function is approximated with the help of the interpolation functions (3) (without any constraints imposed on the number of the element nodes);
b) a control domain, in which the energy is balanced, is created around each of the mesh nodes.

The idea of the method is similar to CVFEM (Control Volume Finite Element Method) [21], however the work [19] and the present paper indicate important discrepancies between both methods. Differences are related to the interpolation of solution of differential equation in finite element and the way the physical values are balanced around mesh node. The following steps of modified elementary balance method are shown in Fig.4.

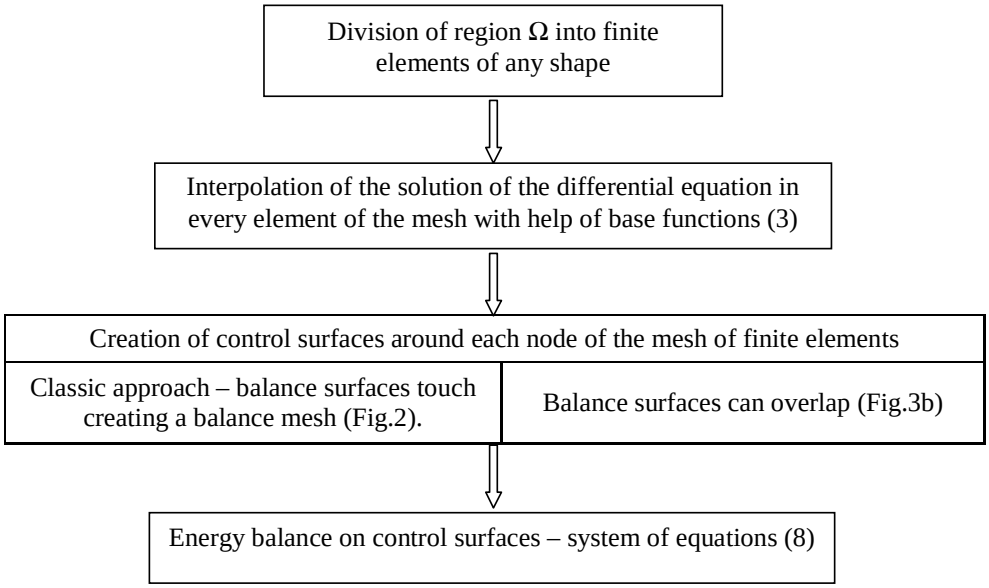

Figure 4: Scheme of generation of system of equations in MCVM.

2. Numerical examples

The MCVM is applied here to solving the direct and inverse problems of ring cooling. Both problems are formulated identically as in [19]:

1. The direct problem – the third kind boundary conditions are given on the inner and outer ring boundaries (Fig.5), i.e. the heat transfer coefficient α (Biot numbers) are known at the ring boundaries

$$\Gamma_o: \quad q_o = -\alpha_o (T_{wo} - T_o), \tag{11}$$

$$\Gamma_i: \quad q_i = -\alpha_i (T_{wi} - T_i), \tag{12}$$

where the index o is related to physical values referring to the outer boundary and the index i to the inner boundary; T_{wo}, T_{wi} – temperature distribution at the ring boundaries.

2. The inverse problem is formulated by temperature and heat flux density distributions at the outer ring boundary (the Cauchy problem for the Laplace equation).

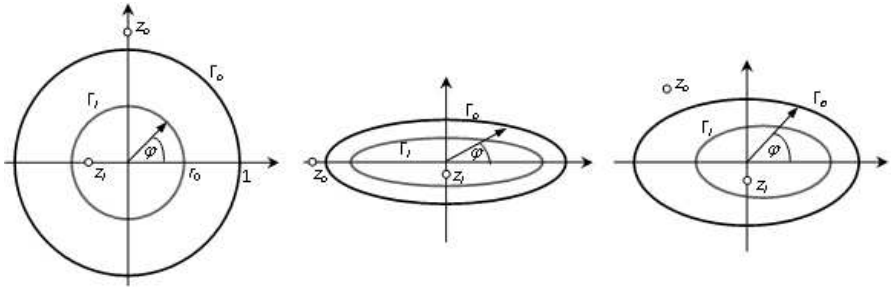

Figure 5: Region Ω: a) circular ring, b) elliptical ring, c) elliptical ring with displaced boundaries.

Example 1

The analytical solution used to compare the calculations performed with this method is expressed by the relationship [1]

$$T(r,\varphi)=T_c+C\cdot \ln r+C\cdot\sum_{m=1}^{\infty}\frac{1}{2m}\left[(ar)^m-\left(\frac{a}{r}\right)^m\right]\cos(m\varphi), \tag{13}$$

where $T_c=T(1,\varphi)$, constant C is equal to the amount of heat transferred through the outer boundary of the ring:

$$C=\int_0^{2\pi}\left[r\frac{\partial T(r,\varphi)}{\partial r}\right]_{r=1}d\varphi .$$

Boundary conditions of a direct problem for the case of C=0.5, a=0.4, T_c=0.9. r_0=0.5 are shown in Fig.6a, while for an inverse one in Fig.6b.

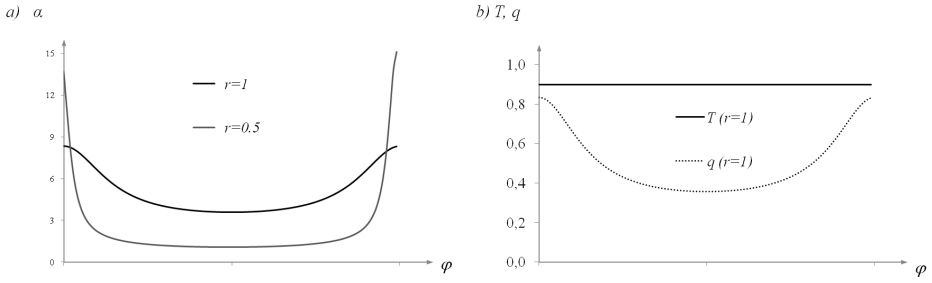

Figure 6: Boundary conditions for a) direct problem – coefficient of heat exchange α on the boundary of the ring and b) inverse problem – temperature and density of heat flux on the outer boundary of the ring. Example 1.

Example 2

Boundary conditions for the circular ring region (Fig.5a) are generated from formula

$$T(r,\varphi) = C_0 + C_1 \cdot ln(z - z_o) + C_2 \cdot ln(z - z_i), \qquad z = re^{i\varphi}, \tag{14}$$

where C_0=0.7. C_1=-0.1. C_2=0.2. $z_o = 1.2 \cdot e^{i\frac{\pi}{2}}$. $z_i = 0.4 \cdot e^{-i\pi}$ (Fig.7).

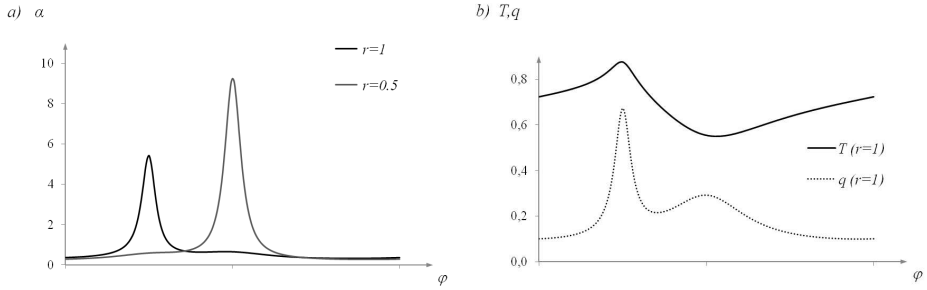

Figure 7: Boundary conditions for a) direct problem – coefficient of heat exchange α on the boundary of the ring and b) inverse problem – temperature and density of heat flux on the outer boundary of the ring. Example 2.

Example 3

Boundary condition for elliptical ring (Fig.5b) boundaries given by equation:

$$\Gamma_o: \quad x^2+\frac{y^2}{0.35^2}=1, \qquad \Gamma_i: \quad \frac{x^2}{0.8^2}+\frac{y^2}{0.2^2}=1,$$

are generated from formula (14) for C_0=0.7. C_1=-0.1. C_2=0.2. $z_o=1.2\cdot e^{i\frac{\pi}{2}}$. $z_i=0.1\cdot e^{-i\pi}$ – (Fig.8).

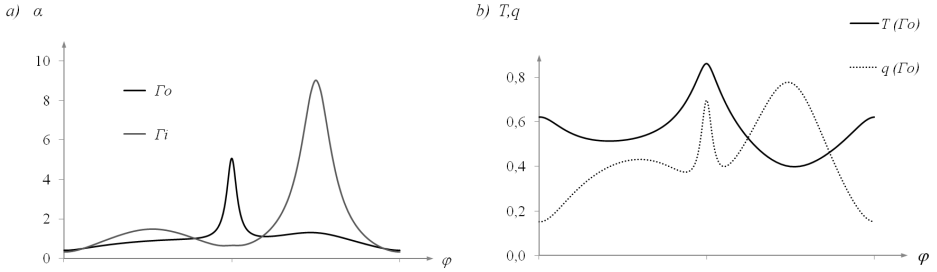

Figure 8: Boundary conditions for a) direct problem – coefficient of heat exchange α on the boundary of the ring and b) inverse problem – temperature and density of heat flux on the outer boundary of the ring. Example 3.

Example 4

Boundary conditions for the elliptical ring with variable thickness region (Fig.5c) and boundaries given by equations:

$$\Gamma_o: \quad x^2 + \frac{y^2}{0.7^2} = 1, \qquad \Gamma_i: \quad \frac{(x-0.1)^2}{0.6^2} + \frac{y^2}{0.4^2} = 1,$$

are generated from formula (14) for C_0=0.7. C_1=-0.1. C_2=0.2. $z_o = 1.2 \cdot e^{i\frac{3\pi}{4}}$. $z_i = 0.3 \cdot e^{-i\frac{\pi}{2}}$, (Fig.9).

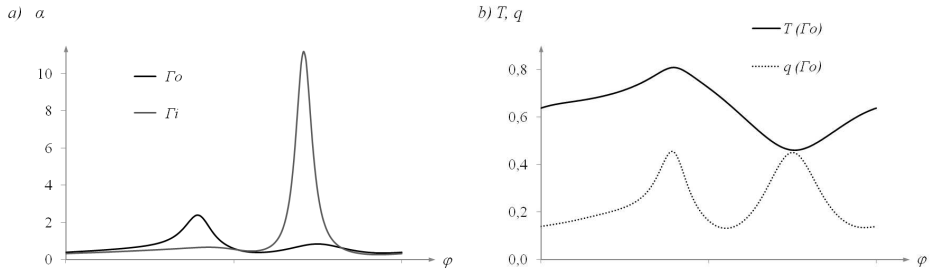

Figure 9: Boundary conditions for a) direct problem – coefficient of heat exchange α on the boundary of the ring and b) inverse problem – temperature and density of heat flux on the outer boundary of the ring. Example 4.

The calculation has been carried out for a six-node element of the triangular mesh and a four-node element of the quadrilateral mesh (Fig. 1) for the interpolation of Solution an element. The parameters of meshes of finite elements used in the particular examples are presented in Table2. The energy balance around each of the mesh nodes provided in both cases the system of equations (10) that was transformed according to temperature and heat flux separation at the outer and inner ring boundaries

$$T_\alpha = \begin{bmatrix} T_{wo} \\ T_{wi} \end{bmatrix}, \qquad Q_\alpha = \begin{bmatrix} q_o \\ q_i \end{bmatrix}$$

- for the direct problem

$$\begin{bmatrix} T_{wo} \\ T_{wi} \end{bmatrix} = \left[B_o + \alpha_o A_o \quad B_i + \alpha_i A_i \right]^{-1} \left[\alpha_o A_o \quad \alpha_i A_i \right] \begin{bmatrix} T_o \\ T_i \end{bmatrix}, \tag{15}$$

- and for the inverse problem

$$\begin{bmatrix} T_{wi} \\ q_i \end{bmatrix} = \left[-B_i \quad A_i \right]^I \left[B_o \quad -A_o \right] \begin{bmatrix} T_{wo} \\ q_o \end{bmatrix}. \tag{16}$$

The formula (16) for the inverse problem contains a pseudo-inverse matrix, determined with the SVD algorithm.

Table 2: Parameters of meshes of finite elements used in the numerical calculations. The number of nodes on the inner boundary of the ring equals the number of nodes on the outer boundary.

Example	Triangular mesh elements			Quadrilateral meshes elements		
	Number of inner nodes	Number of nodes on the boundary	Number of inner nodes	Number of nodes on the boundary	Number of inner nodes	Number of nodes on the boundary
1.	700	200	400	800	200	900
2.	3800	400	2000	3600	400	3800
3.	1400	400	800	1600	400	1800
4.	3800	400	2000	3600	400	3800

The results of calculations for the triangular and quadrilateral meshes in case of the inverse problem of ring cooling are shown in Figs. 10 – 13. The plots are made for the known undisturbed temperature and flux values at the outer ring boundary.

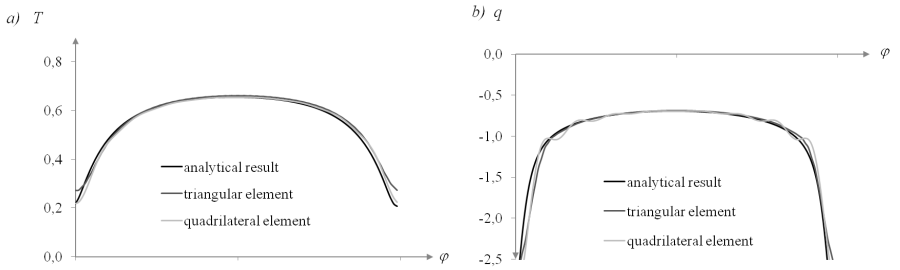

Figure 10: Distribution a) temperature and b) density of heat flux on inner boundary of ring for undisturbed data, f=5 – example 1.

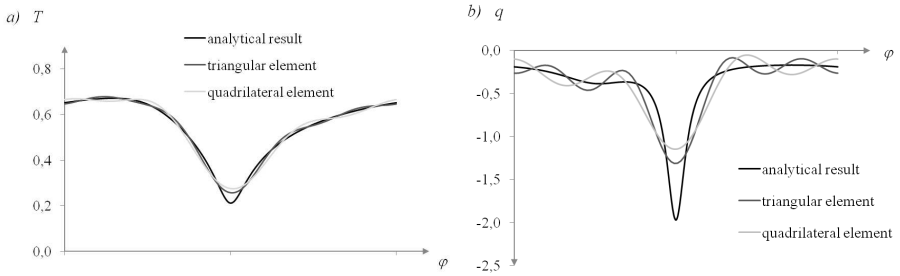

Figure 11: Distribution a) temperature and b) density of heat flux on inner boundary of ring for undisturbed data, f=3 – example 2.

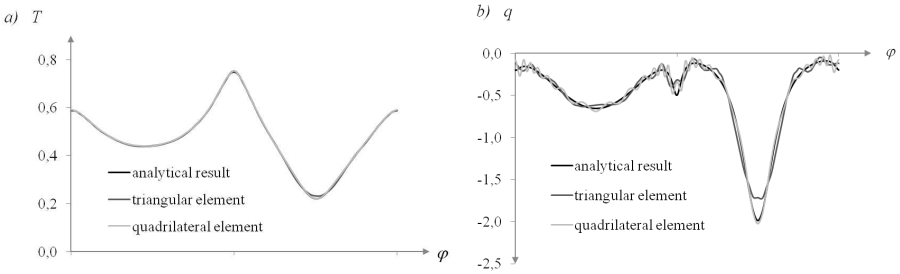

Figure 12: Distributions a) temperature and b) density of heat flux on inner boundary of ring for undisturbed data, f=5 for triangular element and f=3 for quadrilateral element – example 3.

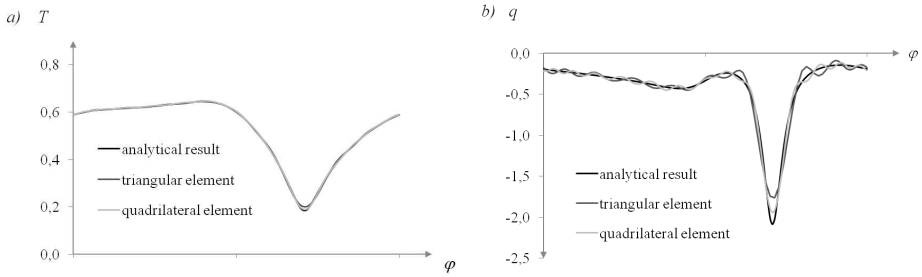

Figure 13: Distribution a) temperature b) density of heat flux on inner boundary of ring for undisturbed data f=3 – example 4.

For estimation both grids, the relative norms [19] have been calculated, which expressed errors of physical value at ring boundary in comparison with analitycal solution

$$\delta L_{2T} = \sqrt{\frac{\int_{\Gamma} (T - T_{analit})^2 ds}{\int_{\Gamma} T_{analit}^2 ds}} \cdot 100[\%], \qquad \delta L_{2q} = \sqrt{\frac{\int_{\Gamma} (q - q_{analit})^2 ds}{\int_{\Gamma} q_{analit}^2 ds}} \cdot 100[\%]. \tag{17}$$

Boundary conditions of both problems are disturbed with the relative error given by the formula

$$\varepsilon = \varepsilon_{max} \cdot (2 \cdot random - 1), \tag{18}$$

where random is for a pseudo-random number in the range (0,1).

In order to minimize the errors of heat flux and temperature at the boundary the patterns of these values have been smoothed by means of linear combination of trigonometric functions [19].

3. Summary

The Tables 3 – 10 show that solution of a direct problem with the use of triangular mesh based on 6 nodes and quadrilateral mesh based on 4 nodes is highly accurate in the sense of the norm (17) with error ε_{max} below 5 per cent, i.e. values of the flux and temperature found in result of the calculation are below 5.5 per cent for temperature, while in case of the flux – below 15 per cent.

The analysis of figures 10-13 and results presented in Tables 3-10 for the numerical examples 1-4 show a significant conformity of the temperature distribution with the analytical solutions for the regularization parameter on algorithm SVD f=3 below 5 % for the error of disturbed of data $\varepsilon_{max}\leq 1\%$. The heat flux on the inner boundary of the ring shows strong oscillations around the analytical solutions for both types of meshes, which leads to a loss of stability of the solution as the maximal error of disturbed data ε_{max} increases. This phenomenon is characteristic for the solution of the inverse problem and it is possible to demonstrate that for the Cauchy problem for a circular ring it is independent for the numerical method of used to solve the problem (an ill-posed problem in Hadamard's sense). A small disturbance in the temperature $T(1,\varphi)$ and heat flux $q(1,\varphi)$ on the boundary Γ_o, lead to a large disturbance of the value of the solution of the Laplace equation on the boundary Γ_i. Let's assume indeed that the disturbances of functions $T(1,\varphi)$ and $q(1,\varphi)$ on the boundary Γ_o are as follows:

$$\delta T(\varphi)=\begin{cases}\varepsilon_{max}\cdot(\pi-\varphi) & 0\leq\varphi\leq\pi\\ \varepsilon_{max}\cdot(\pi+\varphi) & -\pi\leq\varphi\leq 0\end{cases}=\pi\varepsilon_{max}+\frac{\varepsilon_{max}}{\pi}\sum_{m=1}^{\infty}\frac{1-(-1)^m}{m^2}cos(m\varphi)$$

$$\delta q(\varphi)=0$$

and we are able to calculate the values of functional of errors of the solution of the Laplace equation at the boundaries Γ_o i Γ_i:

$$\delta J_o=\frac{1}{2\pi}\int_0^{2\pi}\left[(\delta T)^2+(\delta q)^2\right]d\varphi=\frac{\varepsilon_{max}^2}{2\pi}\left(\pi^2+\sum_{k=1}^{\infty}\frac{1}{(2k-1)^4}\right)$$

$$\delta J_i=\frac{1}{2\pi}\int_0^{2\pi}\left\{\left[\delta T(r_0,\varphi)\right]^2+\left[\delta\frac{\partial T(r_0,\varphi)}{\partial r}\right]^2\right\}d\varphi=$$

$$=\frac{\varepsilon_{max}^2}{2\pi}\left[\pi^2+\sum_{k=1}^{\infty}\left(1+\frac{(2k-1)^2}{r_0^2}\right)\left(r_0^{2k-1}+\frac{1}{r_0^{2k-1}}\right)^2\frac{1}{(2k-1)^4}\right]=\infty$$

The numerical solution has a form of solution in closed form. By analogy to the above result it is possible to make a conclusion that the larger the value of parameter f and error ε_{max}, the larger the value of error of solution.

The calculation results are stable for the small values of the parameter f, which means that the solution of the system of equations (10) was obtained at the border line of the application of the SVD algorithm. This opens the door to the other direction in research where the Tichonow regularization is applied to solve that system of equations or it is solved by the iterative solution of sequence of direct problems.

The smoothness of disturbed data has not influence on value of parameter f only less improve of solution of Cauchy problem for disturbed data.

The calculation results obtained for the two different cases of energy balancing don't differ by much. In the case of the quadrilateral element mesh the control area is generated around the mesh node where the energy balance is performed in a way similar to that used in classical

method of elementary balances (finite volumes), while in case of triangular mesh the control areas around different nodes may interpenetrate. This makes a significant difference with respect to the classical method of elementary balances and CVFEM, as it indicates the way of generalization of the method to the meshes of various shapes.

APPLICATION OF INVERSE PROBLEM OF THE POISSON EQUATION IN THE COOLING PROCESS OF A GAS-TURBINE BLADE

Formulation of the problem

A multiply connected region Ω bounded with the boundary $\Gamma=\Gamma_{out}\cup\Gamma_{in}$ shown in Fig. 1 is distinguished by a complex geometry. The Cauchy problem for the region may be formulated as follows: distribution of temperature and heat flux density at the outer boundary of the gas turbine blade (Fig. 1) are given:

$$T\big|_{\Gamma_{out}} = T_{wout}, \qquad -\lambda\frac{\partial T}{\partial n}\bigg|_{\Gamma_{out}} = q_{out}, \tag{1}$$

the heat flux and temperature distribution are to be found at the inside boundaries Γ_m (in the blade channels) Fig. 1.

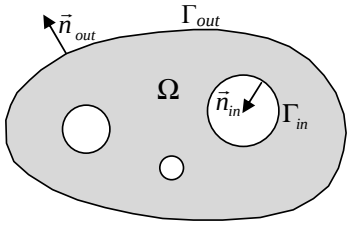

Fig. 1. Multiply connected region Ω bounded with the boundary $\Gamma=\Gamma_{out}\cup\Gamma_{in}$

Such inverse problem formulated this way not always may be solved. Therefore, we look for a solution in the means-square sense:

$$\frac{\partial T}{\partial n}\bigg|_{\Gamma_{out}} = -\frac{q_{out}}{\lambda}, \qquad \frac{1}{2}\int_{\Gamma_{out}}(T-T_{wout})^2\,ds = \min \tag{2a}$$

or

$$\frac{\partial T}{\partial n}\bigg|_{\Gamma_{out}} = \frac{\alpha_{out}}{\lambda}\left(T-T_{gas}\right), \qquad \frac{1}{2}\int_{\Gamma_{out}}(T-T_{wout})^2\,ds = \min. \tag{2b}$$

The method of solving the inverse problem

In the multiply connected region Ω (Fig. 1) the Laplace equation is solved as follows

$$c(z)\cdot T(z)=\oint_{\Gamma} T(\xi)\cdot\frac{\partial \ln|\xi-z|}{\partial n}\cdot d\gamma-\oint_{\Gamma}\frac{\partial T(\xi)}{\partial n}\cdot\ln|\xi-z|\cdot d\gamma \tag{3}$$

where $\xi=\zeta+i\eta\in\Gamma$, $z=x+iy\in\Omega$, and the *c(z)* function is provided by the formula

$$c(z)=\begin{cases}2\pi & z\in\Omega,\\ \gamma & z\in\Gamma,\end{cases} \tag{4}$$

$\gamma=\pi$ for a smooth boundary.

The paper [4] includes a solution to the inverse problem of cooling of a gas turbine blade obtained with the boundary element method. At the Γ boundary *N* points $\xi_1,\xi_2,\ldots,\xi_N$ should be selected, approximating the boundary with piecewise linear lines. Integrals occurring in (3) are determined by approximation of the boundary heat flux and temperature with a linear function. This is described by the equation

$$c(z)\cdot T(z)=\sum_{k=1}^{n}a_k(z)\cdot T_k+\sum_{k=1}^{n}b_k(z)\cdot q_k\ . \tag{5}$$

Substitution of $z=\xi_l\in\Gamma$ into (5) provides a matrix equation reflecting the relationship between the temperature *T* and the heat flux *q* at the Γ boundary

$$\sum_{k=1}^{n}\left[c(\xi_l)\delta_{kl}-a_k(\xi_l)\right]\cdot T_k=\sum_{k=1}^{n}b_k(\xi_l)\cdot q_k\ , \qquad l=1,2,\ldots N, \tag{6}$$

$$Aq=BT\ . \tag{7}$$

If the physical values related to the outer (the "*out*" index) and the inner (the "*in*" index) boundaries are separated, one obtains:

$$\begin{bmatrix}A_{out} & A_{in}\end{bmatrix}\begin{bmatrix}q_{out}\\ q_{in}\end{bmatrix}=\begin{bmatrix}B_{out} & B_{in}\end{bmatrix}\begin{bmatrix}T_{wout}\\ T_{win}\end{bmatrix}, \tag{8}$$

and the solution to the inverse problem in a matrix notation has the following form

$$\begin{bmatrix}T_{win}\\ q_{in}\end{bmatrix}=\begin{bmatrix}-B_{in} & A_{in}\end{bmatrix}^{I}\ \begin{bmatrix}B_{out} & -A_{out}\end{bmatrix}\begin{bmatrix}T_{wout}\\ q_{out}\end{bmatrix}, \tag{9}$$

where T_{out}, T_{in} – temperatures of outer and inner gas, respectively.

Instead of searching the temperature and heat flux at the Γ_{in} boundary we can solve the Poisson equation in the simply connected region bounded with the Γ_{out} boundary. For known boundary conditions (2a) or (2b) we shall search the distribution of the source power in the Ω_{in} regions.

Solution of the Poisson equation in the region bounded with the Γ_{out} boundary and the heat sources located in the Ω_{in} regions is as follows: $c(z)\cdot T(z)=\oint_{\Gamma_{out}} T(\xi)\cdot\frac{\partial \ln|\xi-z|}{\partial n}\cdot d\gamma-\oint_{\Gamma_{out}}\frac{\partial T(\xi)}{\partial n}\cdot\ln|\xi-z|\cdot d\gamma+\int_{\Omega_{in}}\rho(y)\ln|y-z|dy_1dy_2$ (10)

Sformatowano

Sformatowano

where $\xi = \zeta + i\eta \in \Gamma_{out}$, $z = x_1 + ix_2 \in \Omega$, $y = y_1 + iy_2 \in \Omega_{in}$ and the *c(z)* function is provided by the formula (4).

A procedure similar to the one used in the boundary element method and discretization of the Γ_{out} boundary and Ω_{in} regions allow to give the equation (10) the following form:

$$c(z) \cdot T(z) = \sum_{k=1}^{n} a_k(z) \cdot T_k + \sum_{k=1}^{n} b_k(z) \cdot q_k + \sum_{l=1}^{m} d_l(z) \cdot \rho_l \,. \tag{11}$$

For the points $z=\xi_l \in \Gamma_{out}$, l=1,2,…,*n* the equation (11) may be written in the matrix form

$$AT_{wout} = Bq_{out} + C\rho \,, \tag{12}$$

provided that m<n. Unknown distribution of the source power *p* may be finally determined according to the formula

$$\rho = C^{I}\left(AT_{wout} - Bq_{out}\right). \tag{13}$$

Thus, a solution in the mean-square sense is obtained. The solution may be corrected by determining temperature of the Γ_{out} boundary, considering the boundary conditions (2b):

$$\overline{T}_{wout} = \left(A - \frac{\alpha}{\lambda}B\right)^{-1}\left(-\frac{\alpha}{\lambda}BT_{gas} + C\rho\right). \tag{14}$$

Knowing the temperature, the heat flux at the Γ_{out} boundary, and the power of the sources one is able, by solving the Poisson problem in all the Ω_{in} regions, to determine the temperature at the Γ_{in} boundaries and, afterwards, the heat fluxes at the Γ_{in} boundaries. The solution obtained this way belongs to the class of inverse problems since the formula (13) includes a pseudo-inverse matrix.

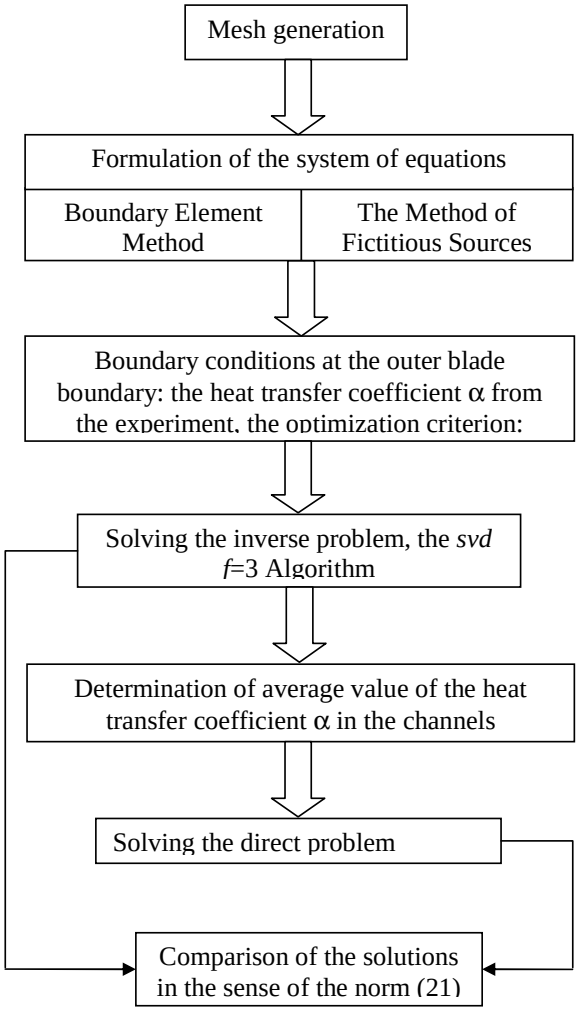

Fig. 2. Optimization scheme of the cooling process of gas turbine blades

Numerical calculation

Solution of the inverse problem provides varying value of the heat transfer coefficient in the channels. Nevertheless, this result does not reflect actual course of the blade cooling process, as in case of its channels a constant values of the heat transfer coefficient α is assumed. In the next optimization step an average α value is determined:

$$\oint_{\Gamma_{in}} q_{in}\,ds = \alpha_{sr} \oint_{\Gamma_{in}} (T_{win} - T_{in})\,ds \quad , \tag{20}$$

where T_{win} – temperature of the blade wall; T_{in} – fluid temperature in the cooling channel. The averaged values of the heat transfer coefficient in the channels determined with the boundary element method and the method of fictitious sources for various temperature values of the outer blade boundary (the optimization criterion) are presented in Table 2.

Values of the heat transfer coefficient in the channels and the distribution of the heat transfer coefficient at the outer blade boundary (Fig. 3) have been used for solving the direct problem with the 3-rd kind boundary conditions. Calculation results for the boundary element method are presented in Figures 5, 6, 7, while for the method of fictitious sources – in Figures 8, 9, 10.

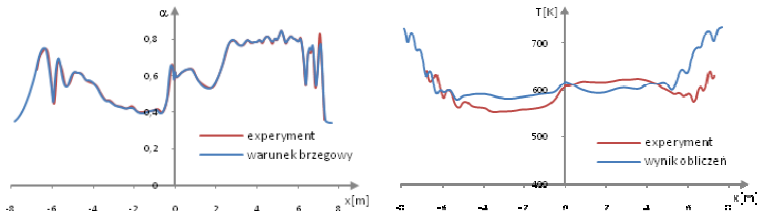

Fig. 3. Distribution of the heat transfer coefficient of the C3X blade (left) and temperature distribution of the C3X blade (right) at the outer surface of the blade, determined experimentally [2]. (RUN 154)

Each of the figures presents the temperature distribution in the blade region and a comparison of the primary temperature distribution at the outer blade surface to the distribution calculated in result of the optimization process. A small difference appears between the distribution so obtained and the one resulting from the optimization criterion.

In order to estimate the quality of the optimization process a relative norm has been assumed

$$N[\%] = \sqrt{\frac{\oint_{\Gamma_{out}} (T_{wout} - T_{opt})^2\,ds}{\oint_{\Gamma_{out}} T_{opt}^2\,ds}} \cdot 100 \quad . \tag{21}$$

Values of the norm for both methods of solving the direct and inverse tasks presented in the paper are shown in Figure 11.

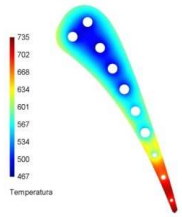

Fig. 4. Temperature distribution of the C3X blade calculated based on the experimental data [2]. (RUN 154)

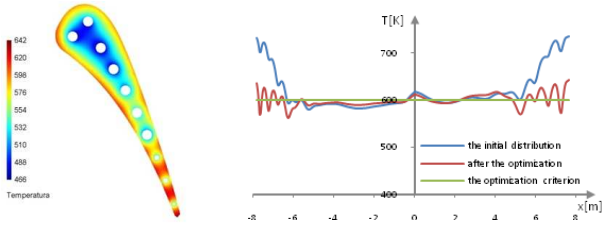

Fig. 5. Temperature distribution of the C3X blade calculated with the Boundary Element Method for the optimization criterion T=600K (left), comparison of temperature distributions at the outer surface of the blade (right)

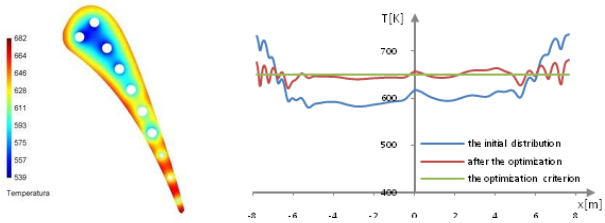

Fig. 6. Temperature distribution of the C3X blade calculated with the Boundary Element Method for the optimization criterion T=650K (left), comparison of temperature distributions at the outer surface of the blade (right)

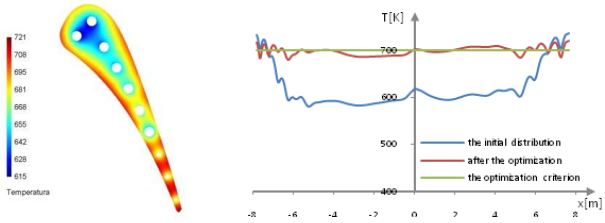

Fig. 7. Temperature distribution of the C3X blade calculated with the Boundary Element Method for the optimization criterion T=700K (left); comparison of temperature distributions at the outer surface of the blade (right)

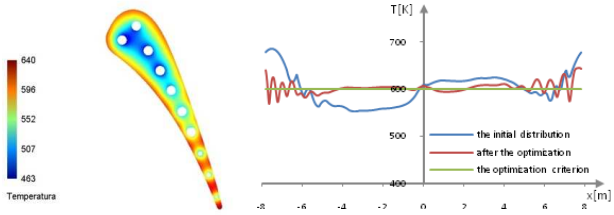

Fig. 8. Temperature distribution of the C3X blade calculated with the method of fictitious sources for the optimization criterion T=600K (left); comparison of the temperature distributions at the outer blade surface (right)

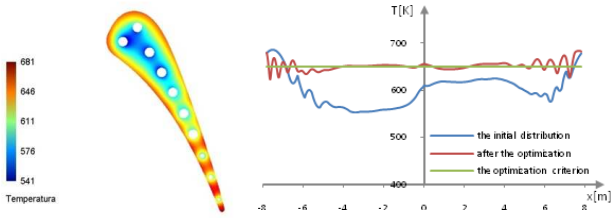

Fig. 9. Temperature distribution of the C3X blade calculated with the method of fictitious sources for the optimization criterion T=650K (left); comparison of the temperature distributions at the outer blade surface (right)

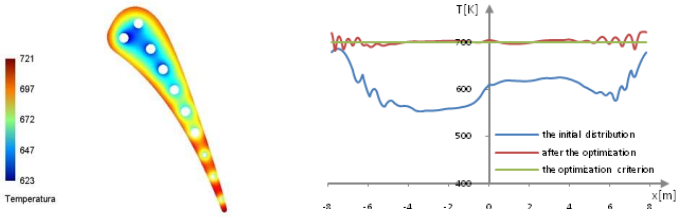

Fig. 10. Temperature distribution of the C3X blade calculated with the method of fictitious sources for the optimization criterion T=700K (left); comparison of the temperature distributions at the outer blade surface (right)

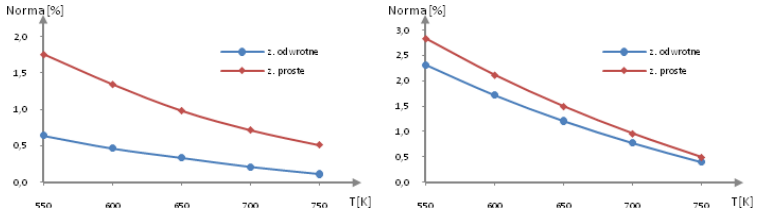

Fig. 11. Comparison of the norms for the inverse and direct problems: the boundary element method (left) and the method of fictitious sources (right).

Table 2. Comparison of heat transfer coefficient values α determined according to the scheme (Fig. 2)

Channel	Primary distribution	Boundary Element Method			The Method of Fictitious Sources (Poisson equation)		
		600[K]	650[K]	700[K]	600[K]	650[K]	700[K]
1	1682	2060	1037	536	2496	1152	570
2	1776	1459	742	497	1052	544	283
3	1827	1748	829	304	1419	697	354
4	1839	1939	857	429	2038	985	497
5	1773	1413	772	426	1390	755	404
6	1327	1404	744	401	1880	989	520
7	1501	2223	1202	650	1434	829	460
8	2092	3094	1675	866	3659	1896	989
9	800	3653	1858	944	4017	1961	994
10	1150	8527	3333	1583	9310	3440	1565

Summary

The essence of the computation presented in the paper consists in testing the Method of Fictitious Sources for the Poisson equation and comparing the results obtained with this method to the ones obtained based on the Boundary Element Method. It should be noticed that solving the inverse problem makes only a part of the optimization scheme of the blade cooling process. As a measure of correctness of the scheme the values of the norm (21) are assumed. It is a relative measure of the distance between the temperature distribution at the outer boundary of the blade and the temperature obtained from the optimization criterion.

Figure 11 shows that the difference between the norm (21) for the direct and inverse problems is smaller for the Method of Fictitious Sources than for the Boundary Element Method, although the norm values are higher. Nevertheless, more important is the fact that the difference in the solution of the inverse problem obtained with the Method of Fictitious Sources and the solution of the direct problem is small. The reason of this is shown in Fig. 12. Distributions of the heat transfer coefficient values in the channels obtained with the Boundary Element Method from the solution of the inverse problem show strong oscillations. In case of the solution of the inverse problem with the Method of Fictitious Sources the oscillations do not appear.

It means that in case of solving the inverse problems related to heat transfer in the blades of channel geometry that precludes the assumption of constant heat transfer coefficient values α the Method of Fictitious Sources described in the present paper directly provides correct (oscillation free) solution to the blade cooling problem.

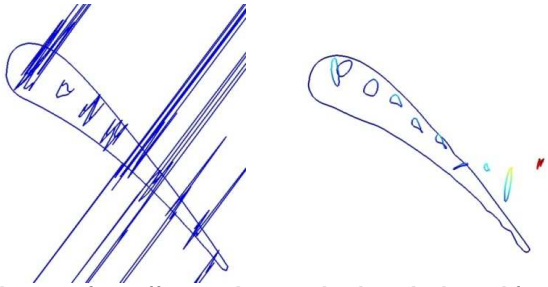

Fig. 12. Distributions of heat transfer coefficient values α in the channels obtained from the inverse problem: with the Boundary Element Method (left) and the Method of Fictitious Sources (right).

INVESTIGATION OF THERMAL LOADING BY SOLUTION OF INVERSE PROBLEM

1. BASIC EQUATIONS

For a one-dimensional transient and linear case the equation of heat conduction is given by:

$$\rho c \frac{\partial T}{\partial \tau} = \lambda \left(\frac{\partial^2 T}{\partial r^2} + \frac{1-2\gamma}{r} \cdot \frac{\partial T}{\partial r} \right) \quad r \in (R_i, R_a), \quad \tau > 0 \tag{1}$$

and after introducing the dimensionless parameters

$$\eta = \frac{r - R_i}{R_a - R_i}, \quad Fo = \frac{\lambda}{\rho c} \cdot \frac{t}{R_a^{\,2}}, \quad \vartheta = \frac{T}{T_0} \tag{2}$$

$$\frac{\partial \vartheta}{\partial F_0} = \frac{\partial^2 \vartheta}{\partial \eta^2} + \frac{1-2\gamma}{\eta + \dfrac{R_i}{R_a - R_i}} \cdot \frac{\partial \vartheta}{\partial \eta}, \qquad Fo > 0, \quad \eta \in (0,1) \tag{3}$$

$$\gamma = \begin{cases} -\dfrac{1}{2} & \text{spherical shell} \\ 0 & \text{cylindrical shell} \\ \dfrac{1}{2} & \text{flat plate} \end{cases} \tag{4}$$

The following conditions are assumed:

– Initial condition

$$\vartheta(\eta, 0) = \vartheta o(\eta), \quad \eta \in \langle 0,1 \rangle \tag{5}$$

– Boundary condition on the surface η=1

$$-\left. \frac{\partial \vartheta(\eta, Fo)}{\partial \eta} \right|_{\eta=1} = Biot\_a\left(\vartheta(1, Fo) - \vartheta_{fluid\_a}^{(Fo)}\right), \quad Fo > 0 \tag{6}$$

In case of the inverse problem measured temperatures in selected points $\eta_k^* = 1,2,...,M\_stern$ in the interior of the body are available instead of boundary conditions on the surface η=0 (r = R_i).

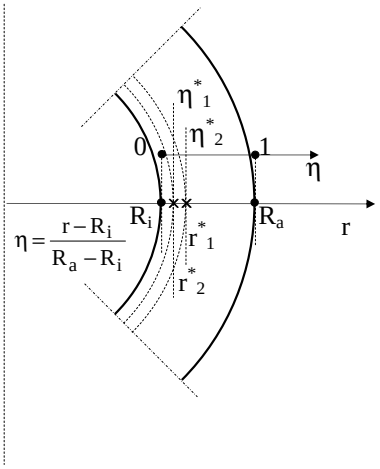

Fig.1. Calculation domain

$$\vartheta\left(\eta_k^*, Fo\right) = \vartheta_k^*(Fo), \quad k = 1,2,...,M\_stern \tag{7}$$

The temperature trend in the point $\eta = 0$ (r = R_i, inner surface) is required. A problem defined this way is called an inverse problem.

2. SOLUTION OF THE INVERSE PROBLEM

In this paper an idea is presented to solve the inverse problem based on the ambition to find a solution that is a least two times differentiable in space. This attribute offer both the Green function method and the solution with spline functions.

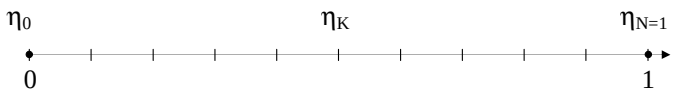

Fig. 2. Grid for interpolation of spline functions

The solution of equation (3) can be expressed as a linear combination of spline functions

$$\vartheta(\eta, \mathrm{Fo}) = \sum_{j=0}^{N} \vartheta(\eta_j, \mathrm{Fo}) \cdot \varphi_j(\eta), \quad \varphi_j(\eta) \in C^2(\langle 0,1 \rangle) \tag{8}$$

For further calculation we introduce the discretization of the first derivative $\partial\vartheta/\partial\mathrm{Fo}$ with a backward quotient

$$\frac{\partial\vartheta}{\partial\mathrm{Fo}} = \frac{\vartheta(\eta, \mathrm{Fo}) - \vartheta(\eta, \mathrm{Fo} - \Delta\mathrm{Fo})}{\Delta\mathrm{Fo}} = \frac{\vartheta - Q}{\Delta\mathrm{Fo}}, \quad Q = \vartheta(\eta, \mathrm{Fo} - \Delta\mathrm{Fo}) \tag{9}$$

so that equation (3) gets the following form

$$\frac{d^2\vartheta}{d\eta^2} + \frac{1-2\gamma}{\eta + a} \cdot \frac{d\vartheta}{d\eta} - \frac{1}{\Delta\mathrm{Fo}} \cdot \vartheta = -\frac{1}{\Delta\mathrm{Fo}} \cdot Q, \qquad a = \frac{R_i}{R_a - R_i} \tag{10}$$

or

$$\frac{d^2\vartheta(\eta)}{d\eta^2} + \frac{1-2\gamma}{\eta + a} \cdot \frac{d\vartheta(\eta)}{d\eta} - \beta^2 \cdot \vartheta(\eta) = -\beta^2 Q(\eta), \quad \eta \in (0,1), \quad \beta^2 = \frac{1}{\Delta\mathrm{Fo}} \tag{11}$$

The solution of equation (10) with spline functions (8) for a constant time step $\Delta\mathrm{Fo}$ is given by

$$\vartheta^n(\eta) = \vartheta(\eta, Fo_n) = \sum_{j=0}^{N} \vartheta_j \cdot \varphi_j(\eta) = \{\varphi\}^T \{\vartheta\}, \quad Fo_n = (n-1)\cdot \Delta Fo, \quad n = 1,2,... \tag{12}$$

The unknown coefficients ϑ_j for each time step are determined by boundary conditions (6), measured temperature distribution (7) and the satisfaction of equation (3) at inner points η_1, η_2, ... η_{N-1}.

The solution of equation (11) at inner points $\eta_1, \eta_2, \ldots, \eta_{N-1}$ gives the following equation

$$\left\{\varphi''(\eta_k) + \frac{1-2\gamma}{\eta_k + a}\cdot\varphi'(\eta_k) - \beta^2 \cdot \varphi(\eta_k)\right\}^T \cdot \{\vartheta\} = -\beta^2 \cdot Q_k, \quad k = 1,2,..., N-1 \tag{13}$$

Next are obtained from the boundary condition (6) und measured temperature trends (7)

$$\{\varphi'(\eta = 1) + Biot\_a \cdot \varphi(1)\}^T \{\vartheta_n\} = Biot\_a \cdot \vartheta_{fluid\_a} \tag{14}$$

$$\{\varphi(\eta_k^*)\}^T \{\vartheta_n\} = \vartheta^*, \quad k = 1,2,\ldots, M\_stern \tag{15}$$

Equations (13) to (15) form a system of linear equations that can be expressed in a matrix:

$$\begin{bmatrix} \{\psi(\eta_1)\}^T \\ \{\psi(\eta_2)\}^T \\ \ldots\ldots\ldots\ldots \\ \{\psi(\eta_k)\}^T \\ \ldots\ldots\ldots\ldots \\ \{\psi(\eta_{N-1})\}^T \\ \{\varphi'(1) + Biot\_a \cdot \varphi(1)\}^T \\ \{\varphi(\eta_1^*)\}^T \\ \ldots\ldots\ldots\ldots \\ \{\varphi(\eta_{M\_stern}^*)\}^T \end{bmatrix} \cdot \begin{Bmatrix} \vartheta_0 \\ \vartheta_1 \\ \vdots \\ \vdots \\ \vdots \\ \vdots \\ \vdots \\ \vdots \\ \vdots \\ \vartheta_N \end{Bmatrix} = \begin{Bmatrix} -\beta^2 \cdot Q_1 \\ -\beta^2 \cdot Q_2 \\ \vdots \\ \vdots \\ \vdots \\ -\beta^2 \cdot Q_{N-1} \\ 0 \\ 0 \\ 0 \\ 0 \end{Bmatrix} + \begin{Bmatrix} 0 \\ 0 \\ \vdots \\ \vdots \\ 0 \\ 0 \\ Biot\_a \cdot \vartheta_{fluid\_a} \\ \vartheta_1^* \\ \vdots \\ \vartheta_{M\_stern} \end{Bmatrix} =$$

$$= \begin{bmatrix} 0 & -\beta^2 & & & & \\ \vdots & & -\beta^2 & & & \\ \vdots & & & & 0 & \\ \vdots & & & & 0 & \\ 0 & & & -\beta^2 & 0 & \\ 0 & & & & 0 & \\ & & & & & \\ 0 & & & & 0 & \\ 0 & & & & 0 & \end{bmatrix} \cdot \begin{Bmatrix} Q_0 \\ Q_1 \\ \vdots \\ \vdots \\ \vdots \\ \vdots \\ \vdots \\ Q_{N-1} \\ Q_N \end{Bmatrix} + \begin{Bmatrix} 0 \\ 0 \\ \vdots \\ \vdots \\ 0 \\ Biot\_a \cdot \vartheta_{fluid\_a} \\ \vartheta_1^* \\ \vdots \\ \vartheta_{M\_stern} \end{Bmatrix} \tag{16}$$

or in a compact form

$$[\psi\_\varphi]\{\vartheta\} = [\beta\_q]\{Q\} + \{FR\} \tag{17}$$

$$\dim[\psi\_\varphi] = (N + M\_stern) * (N+1), \quad \dim[\beta\_q] = (N + M\_stern) * (N+1)$$

And the solution of equation (17) can be written in a symbolic form:

$$\{\vartheta\} = [\psi\_\varphi]^I [\beta\_q]\{Q\} + [\psi\_\varphi]^I \{FR\} \tag{18}$$

where $[\psi\_\varphi]^I$ is a pseudo-inverse matrix (if N + M_stern > N + 1).

3. STABILITY ANALYSIS OF THE INVERSE MATRIX

Stability analysis is based on equation (18). The vector $\{\vartheta\}$ is known for the time Fo_n and the vector $\{Q\}$ is known for the time Fo_{n-1}. With the assumption of $\vartheta(\eta, Fo_n) = \vartheta^n(\eta)$, $\vartheta(\eta, Fo_{n-1}) = \vartheta^{n-1}(\eta) = Q(\eta)$ equation (18) can be expressed in the following form

$$\left\{\vartheta^n\right\} = [STAB] \cdot \left\{\vartheta^{n-1}\right\} + [\psi\_\varphi]^I \left\{FR^n\right\}, \quad n = 1,2,3,\ldots \tag{19}$$

with $[STAB] = [\psi\_\varphi]^I \cdot [\beta\_q]$ as stability matrix of the inverse problem. The solution of equation (3) is stable if the spectral radius $\rho_s([STAB])$ satisfies the inequality $\rho_s < 1$. The spectral radius depends on the time step ΔFo, the node distribution η_k, k = 0,…, N, (Fig. 2) and the number of nodes N. The temperature distribution for the current time step Fo_n is influenced by the measured temperatures $\vartheta_1^*,\ldots,\vartheta_{M-stern}^*$ at inner points $\eta_1^*,\ldots,\eta_{M-stern}^*$ which is included in the vector $\{FR^n\}$. Assuming that the vector $\{FR^n\}$ is disturbed by the term $\{\delta F\}^n$ and the vector of initial temperature $\left\{\vartheta^0\right\}$ is I disturbed by the term $\left\{\delta\vartheta^0\right\}$ the following equations can be written for the first three time steps

$$\left\{\vartheta^1\right\} = [STAB]\left\{\vartheta^0\right\} + [\psi\_\varphi]^I \cdot \left\{FR^1\right\}$$

$$\left\{\vartheta^2\right\} = [STAB]\left\{\vartheta^1\right\} + [\psi\_\varphi]^I \cdot \left\{FR^1\right\} = [STAB]^2\{\vartheta\} + [STAB][\psi\_\varphi]^I \left\{FR^1\right\} + [\psi\_\varphi]^I \left\{FR^2\right\}$$

$$\left\{\vartheta^3\right\} = [STAB]\left\{\vartheta^2\right\} + [\psi\_\varphi]^I \cdot \left\{FR^3\right\} =$$

$$= [STAB]^3\left\{\vartheta^0\right\} + [STAB]^2[\psi\_\varphi]^I \left\{FR^1\right\} + [STAB][\psi\_\varphi]^I \left\{FR^2\right\} + [\psi\_\varphi]^I \left\{FR^3\right\}$$

and for arbitrary time steps

$$\left\{\vartheta^n\right\} = [STAB]^n \left\{\vartheta^0\right\} + \sum_{k=0}^{n-1} [STAB]^k \cdot \left\{FR^{n-k}\right\} \tag{20}$$

and for the disturbed data

$$\left\{\vartheta^n + \delta\vartheta^n\right\} = [STAB]^2 + \left\{\vartheta^0 + \delta\vartheta^0\right\} + \sum_{k=0}^{n-1} [STAB]^k \cdot \left\{FR^{n-k} + \delta FR^{n-k}\right\} \tag{21}$$

Subtraction equation (21) from equation (20) gives an disturbed vector as a function of the interfered initial temperature und and the disturbed measured temperature for every time step including the current one.

$$\left\{\delta\vartheta^{n}\right\} = [\mathrm{STAB}]^{n} \cdot \left\{\delta\vartheta^{o}\right\} + \sum_{k=0}^{n-1} [\mathrm{STAB}]^{k} \cdot \left\{\delta \mathrm{FR}^{\,n-k}\right\} \tag{22}$$

From equation (22) results that damping of measurement errors is increasing with a decreasing spectral radius ρ_s of the stability matrix [STAB] and satisfies the inequation $\rho_s < 1$.

4. NUMERICAL CALCULATION

The spectral radius ρ_s of the stability matrix [STAB] (20) plays a decisive role for the convergence of the inverse problem. If $\rho_s < 1$ the solution of equation (19) is convergent. Figure 3 shows the dependence of the spectral radius from the time step for different values of heat transfer coefficient on the outer surface. Higher values of the heat transfer coefficient (at the surface $r = R_a$) correspond to lower spectral radii and the spectral radius decreases with increasing time steps.

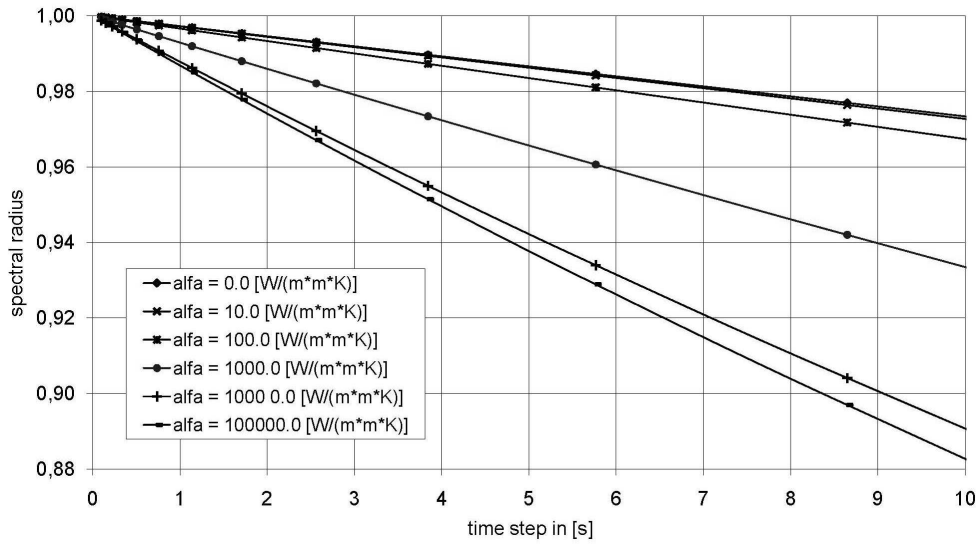

Fig. 3. Spectral radii as a function of time step for different heat transfer coefficients

To verify the presented method to solve the inverse problem the temperature distribution at inner points of the cylindrical wall are generated from the analytical solution (direct problem). Figure 4, 5 and 6 show the calculated heat transfer coefficient on the inner surface as solution of the inverse problem. The calculation is based on a cylindrical geometry with R_i = 100 mm and R_a = 180 mm. Results from the inverse calculation are in good agreement with the given values for the direct solution. The error rate of the solution reaches values of approx. 1% for the heat transfer coefficient α = 5000 W/m²K and of less that 1% for lower heat transfer coefficients.

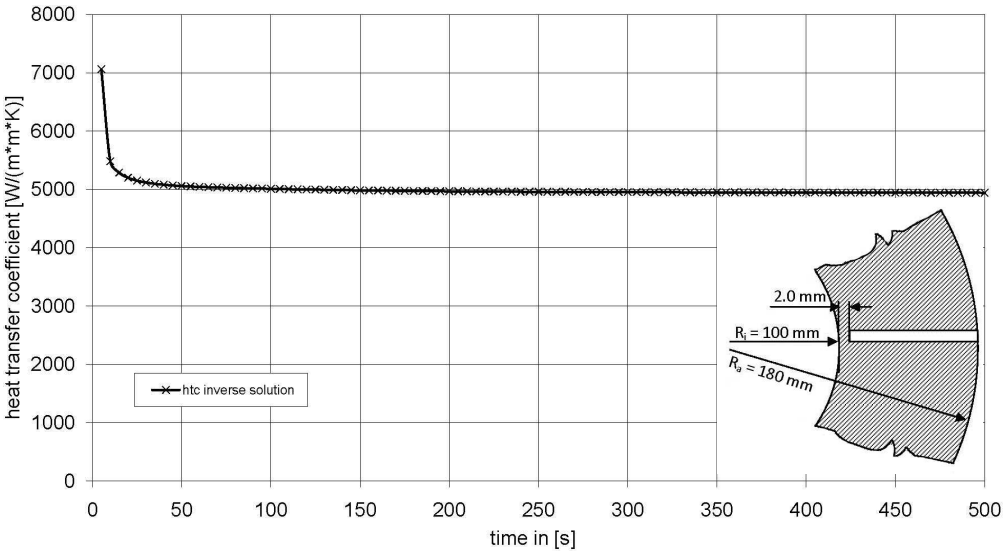

Fig. 4. Solution of inverse problem with exact data from direct problem with α = 5000 W/m²K

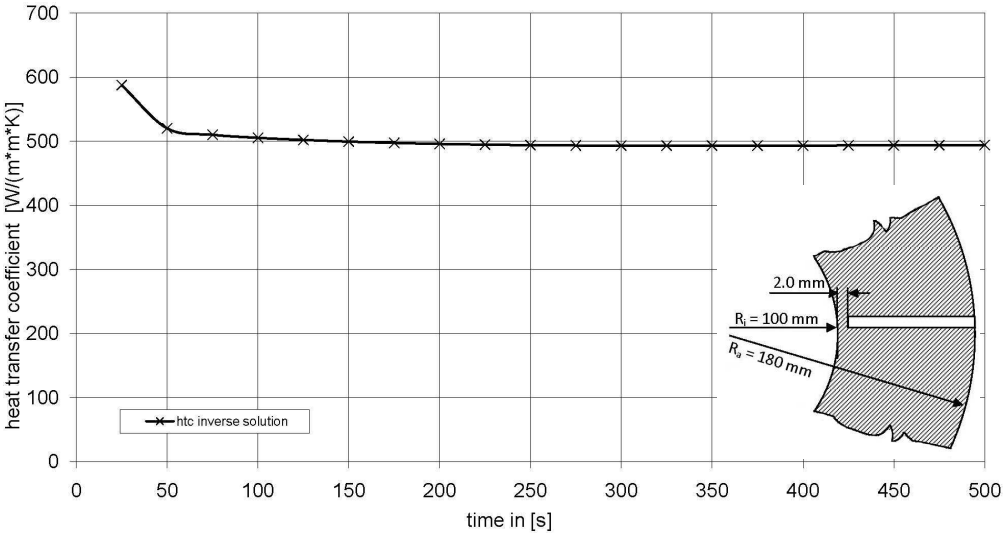

Fig. 5. Solution of inverse problem with exact data from direct problem with α = 500 W/m²K

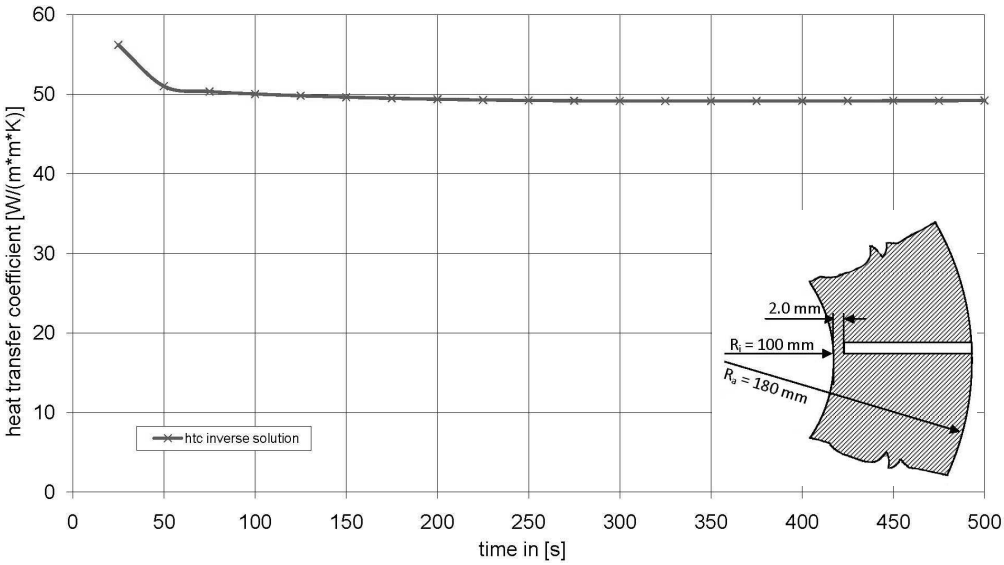

Fig. 6. Solution of inverse problem with exact data from direct problem with $\alpha = 50$ W/m²K

In a second step measured temperatures from a steam turbine casing were used to calculate the heat transfer coefficients on the inner surface (steam touched) using the presented inverse method. Figure 7 shows the calculated heat transfer coefficient inside of an exhaust steam casing. Fluid and wall temperatures are comparatively low due to vacuum conditions. The structure is considered as a cylinder with inner radius R_i = 560 mm and outer radius R_a = 582 mm. Two thermocouples are located 2.2 mm and 11.6 mm from the inner surface. The outer surface is in contact with ambient air. Fluid temperature is set to 30°C and the heat transfer coefficient to 20 W/m²K. The peak in the calculated heat transfer coefficient at approximately 250 seconds results from wall condensation that increases the heat transfer drastically.

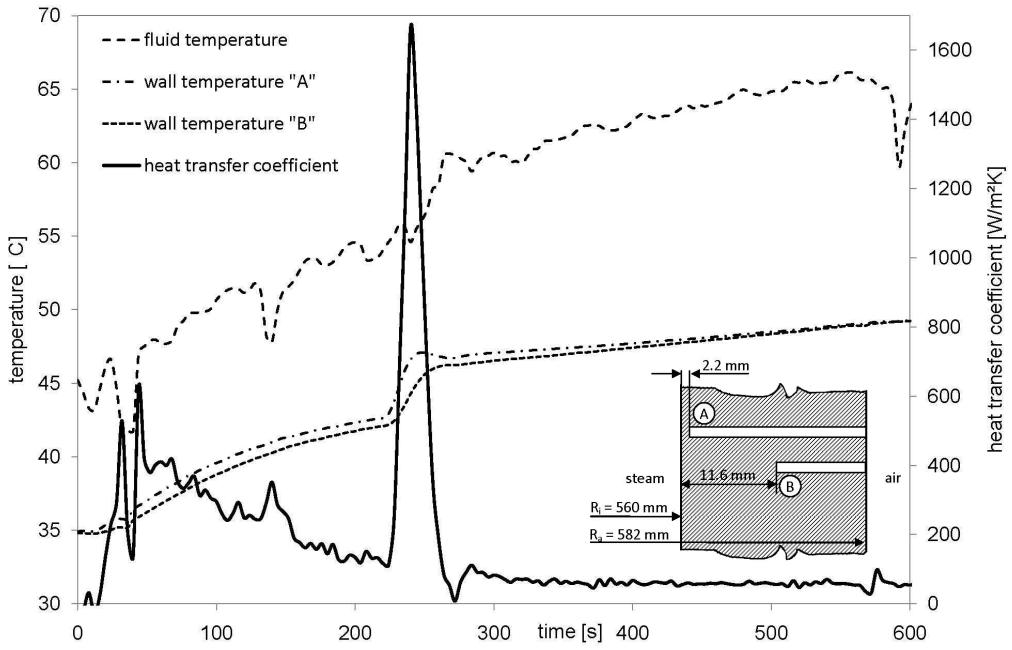

Fig. 7. Solution of inverse problem using measured temperatures taken at exhaust steam casing

Figure 8 shows the calculated heat transfer coefficient inside the inlet section of a steam turbine casing. The turbine was operated on a test rig with reduced steam temperatures and pressures. This inlet section can be considered as a horizontal pipe with inner radius R_i = 100 mm and outer radius R_a = 180 mm. Boundary conditions on the outside surface were chosen as fluid temperature 30°C and heat transfer coefficient 20 W/m²K. The heat transfer coefficient reaches maximal values of 18000 W/m²K which is a result of high velocity steam flow and wall condensation.

In case of the inlet section of the steam turbine the structure is considered as a cylinder because the relative wall thickness $(R_a - R_i) / R_a = 0.44$ is comparatively high. When this structure is calculated as a flat plate with identical wall thickness the heat transfer coefficient changes considerably, as shown in Figure 9. This clearly reveals that a structure like the inlet section should not be considered as a plate. For the exhaust steam casing (Fig. 7) the relative wall thickness is only 0.03 and if the cylinder is considered as a flat plate the calculated heat transfer coefficients are practically identical.

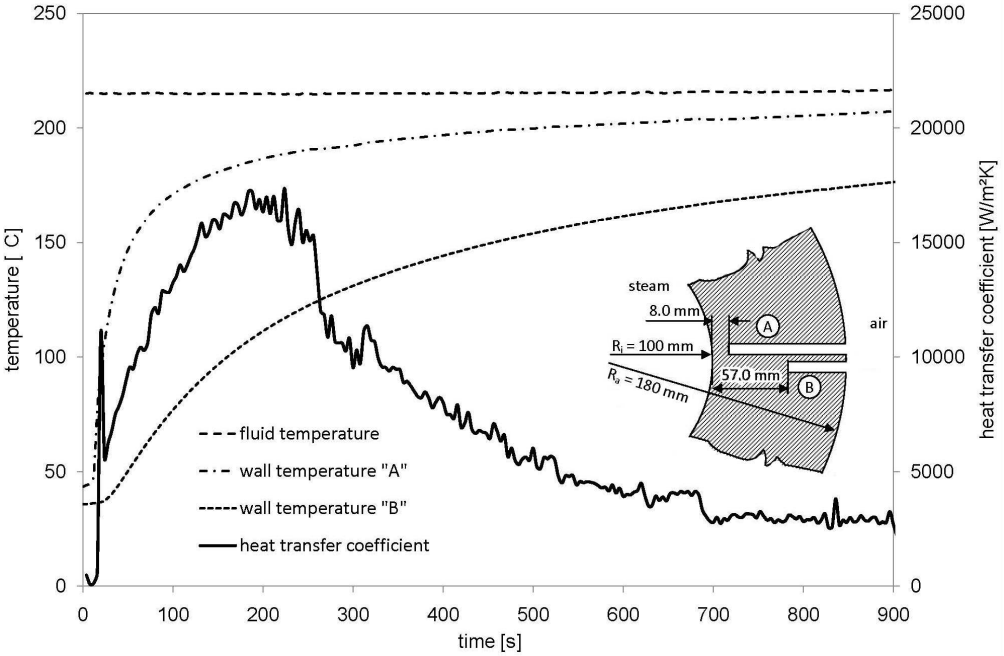

Fig. 8. Solution of inverse problem using measured temperatures taken at inlet of steam turbine casing

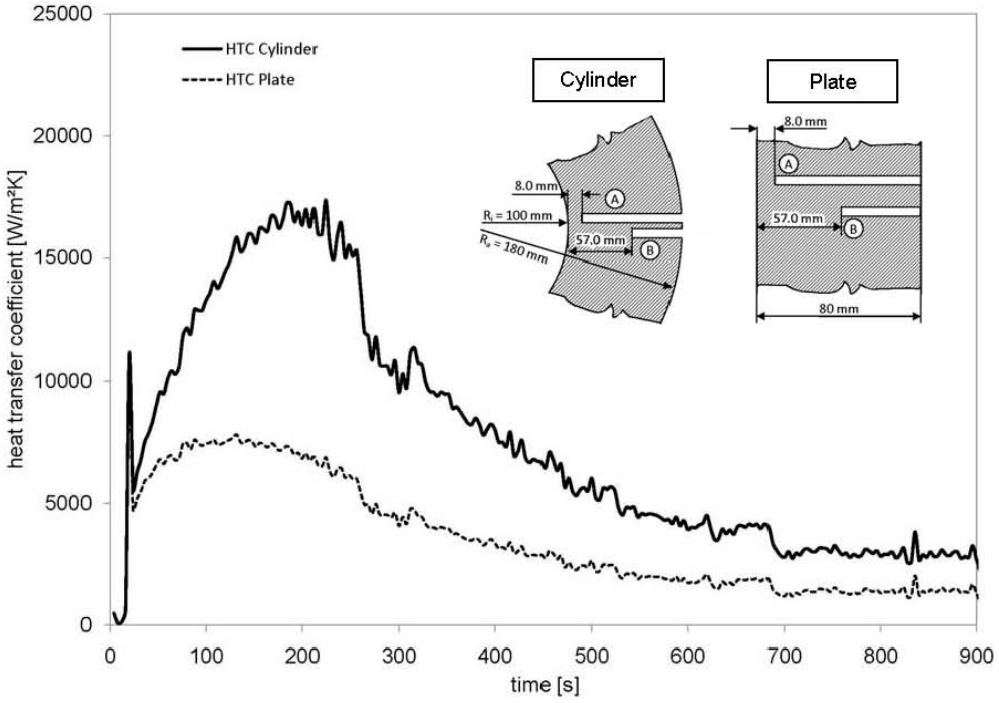

Fig. 9. Solution of inverse problem calculated for cylinder and flat plate with identical wall width

5. FINAL REMARKS

Investigation of thermal loading of elements of thermal machines is necessary for appropriate its exploitation (protection before pass of allowable thermal stresses). On account of exploitation of thermal machines it is impossible measurement of temperature at inner surface of machine but is possible in some distance from this surface. Determination temperature at inner surface leads to the inverse problem. For solution of inverse problem authors applied discretization of heat conduction equation (1) with respect to time variable and solution with respect to space variable was assumed as linear combination of hyperbolic spline functions [27] (usually spline functions lead to non-stable solution of inverse problem). Obtained solution of inverse problem is stable and very accurate what proves comparison tests for different values of heat transfer coefficients. Presented method is appropriate for permanent monitoring state of thermal loading in real time. Spline function method will be used by authors for case when coefficient of thermal conductivity, density, and specific heat are function of temperature what requires solution of non-linear Eq. (17).

INVERSE SOURCE PROBLEM

Solution to the problem „Flow in a cavity" through solution of inverse source problem for heat conduction equation

Motion of 2D incopressible viscous flow is described by the equation with stream function Ψ

$$\frac{\partial}{\partial t}\Delta\Psi - \nu\Delta\Delta\Psi = \frac{\partial\Psi}{\partial x}\cdot\Delta\frac{\partial\Psi}{\partial x} - \frac{\partial\Psi}{\partial y}\cdot\Delta\frac{\partial\Psi}{\partial x}$$

or by acting with inverse operato Δ^{-1} , the motion equation is transfrmed into heat condction equation with unknown harmonic source function

$$\frac{\partial}{\partial t}\Psi - \nu\Delta\Psi = \Delta^{-1}\left(\frac{\partial\Psi}{\partial x}\cdot\Delta\frac{\partial\Psi}{\partial x} - \frac{\partial\Psi}{\partial y}\cdot\Delta\frac{\partial\Psi}{\partial x}\right) + H(x,y,t), \qquad \Delta H \equiv 0$$

the solution of motion equation is equivalent to the solution to the inverse source problem for heat conduction equaton

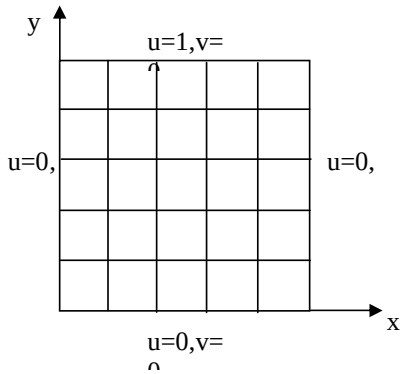

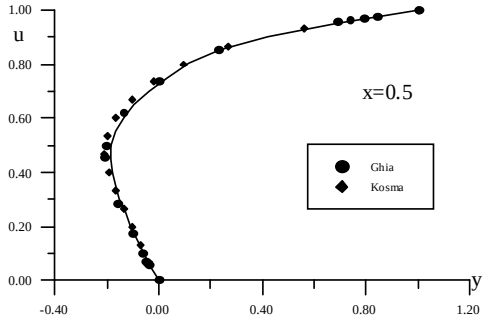

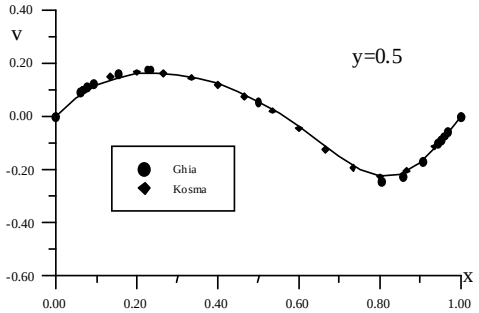

Thank you for your attention.